ELECTRONIC DETECTOR FOR PERFORMING THE S-16 PARTICLE ASYMMETRY EXPERIMENT ON AAP MISSIONS

Final Report

Study period: 7-1-67 through 4-30-68

Contract: NAS 9-5249

Personnel: Harry Heckman, Project Director

Douglas Greiner, Physicist

Richard Albert, Physicist

Peter Lindstrom, Programmer

Frederick Bieser, Electronics Engineer

Sub Contract: Lawrence Radiation Laboratory

Electronic Engineering Research and Development

Fred S. Goulding in charge

NASA CR 92120

CONTENTS

I. INTRODUCTION

The S-16 Particle Asymmetry experiment, as originally conceived, involved the use of nuclear emulsion detectors that were to be magnetically oriented during periods of irradiation to energetic protons in the region of the South Atlantic anomaly. However, owing to the cancellation of the AS 205 and AAP-1A missions, each of 14-day duration, the S-16 experiment has not been performed. On the basis of present planning, future AAP-type missions are to be of longer flight duration than 14 days, typically 28 to 56 days at altitudes about 250 n mi. Flights of this duration and altitude preclude the use of emulsions for this experiment because of the excessive exposure to the trapped particles the emulsion will receive, making the data analysis difficult, if not impossible.

As an alternative approach for carrying out the S-16 experiment, we have undertaken this study to design and develop an "S-16" electronic, solid-state counter telescope. The features of this counter are sufficiently comprehensive as to mass, energy and angular resolution so that it can be employed in future Apollo earth-orbital missions in order to obtain trapped particle data that can meet the objectives of the Particle Asymmetry experiment.

Due to the cancellation of the AAP Mission, 1A, we shall not include feasibility studies for carrying out emulsion experiments on missions in excess of 14 days as are now planned. The inherent difficulties of over-exposure of the emulsion detectors incurred on such missions do not make such studies particularly valuable. We shall, therefore, concentrate on Section B of the Statement of Work, which was the basic

objective of this study. This section of the Statement of Work is as follows:

Generate conceptual design sketches and mockups describing the changes required to meet experiment objectives and spacecraft interfaces.

1. Investigate feasibility of utilizing electronic sensors in place of nuclear emulsion.

2. Determine telemetry and/or data recording requirements for electronic sensors.

3. Construct a breadboard model of electronic sensor to demonstrate functional operations.

II. THE S-16 PARTICLE ASYMMETRY EXPERIMENT: A SUMMARY

The purpose of the S-16 experiment was to study the spectrum and flux asymmetries in the proton component of the geomagnetically trapped radiation in the South Atlantic anomaly. As originally conceived, the experiment would employ a magnetically oriented nuclear emulsion package that would be exposed to the trapped radiation outside the Apollo spacecraft whenever the spacecraft traversed the South Atlantic anomaly. The experiment was specifically conceived for an earth-orbital mission such as the Apollo.

The principal objectives of the S-16 experiment were:

a) To measure the Van Allen proton spectrum to as low as 2-5 MeV.

b) To measure the directional differential energy spectra for trapped protons. It is from the differences between the directional spectra that the east-west asymmetries, hence the scale height of the atmosphere, are obtained.

c) To measure the proton pitch-angle distribution. An accurate measurement of this distribution will yield the altitude dependence of the flux for lower altitudes.

d) To search for trapped particles heavier than protons, e.g., deuterons, tritons, and, most important, alpha particles, which have not yet been observed.

The S-16 experiment was to form part of a continuing study by the investigator on the proton component of the trapped radiation at low satellite altitudes.[1-4] Had the S-16 experiment been performed during the A/S 205 mission, with a follow-on for AAP-1A, our observations would have been extended to the years 1968-70. Data received during this time

interval would have been particular important to our basic research effort since this will be the period of maximum solar activity when significant changes in the trapped radiation are expected.[5] The most appropriate region to observe such variations is in the region of the South Atlantic anomaly where the mirror-point trajectories of the trapped radiation reach their minimum altitudes.

The basic objective of the S-16 experiment was, thus, to obtain information on the processes by which protons are injected, trapped and lost from the inner radiation belt, and their changes during the solar-cycle period.

The emulsion experiment of Freden and White[6] first showed that the penetrating components of the inner radiation belt are high energy protons. They found that between 75 MeV and 600 MeV the proton energy spectrum was of the form $N(E)\,dE \propto E^{-1.8}\,dE$. Later, measurements of the proton energy spectrum over similar ballistic trajectories extended the spectrum to as low as 12 MeV.[1] The notable feature of the inner proton belt is its remarkable temporal stability as to flux and energy spectra. Exceptions to this observation were made by Explorer VII[7] and Relay I[8] experiments when changes in the distribution of the inner belt protons were affected by magnetic disturbances. Only recently have solar cycle changes been evident.[4] The time and altitude dependence (1961 through 1964) of the 55 MeV proton flux at low altitudes, as observed in the emulsion experiments of Filz and Holeman,[9] result in the conclusion that a large increase in the proton flux occurred at the time of Starfish due to a redistribution of pitch angles. Such an effect may account for an increase of a factor of four in the flux between the times of the Explorer IV (1958)[10] and Injun 3 (1963)[11] measurements.

Recently, improved theoretical calculations on the trapped proton flux from cosmic ray and solar proton albedo neutron decay have been carried out by Dragt, et al.[12] and Hess and Killeen.[13] They conclude from their calculations that only 2 to 3 percent of the observed proton flux is accounted for at high B values (low altitudes)! The nature and strength of the source of the inner proton belt is clearly less understood than was once believed.

Since September, 1962, the investigator, in cooperation with G. H. Nakano, has been carrying out a systematic nuclear emulsion study of the trapped protons, $E > 58$ MeV, over the South Atlantic.[2,3,4] The analysis of the emulsions recovered from oriented polar-orbiting satellites (altitudes 400 ± 100 km) after 2-6 days in orbit has yielded the following results.

a) The angular distribution of the mirroring protons about a normal to the magnetic field is approximately Gaussian with a standard deviation of $\approx 7^{\circ}$.

b) The variation of proton flux vs altitude is entirely consistent with atmospheric losses.

c) An east-west asymmetry in the proton flux has been observed and effective atmospheric scale heights calculated therefrom. These results are in agreement with scale heights deduced from satellite data.

d) The shape of the proton spectra between 58 and 600 MeV has not changed, within the accuracy of measurement, since 1962; -- nor, in fact, upon comparison with earlier energy spectra measurements, since 1958-9.

e) The flux of 63 MeV protons has decreased by a factor of 2 (as of January 1968) relative to the flux observed during the period of

solar minimum. Such a flux change is consistent with atmospheric heating and, hence, density changes, owing to increasing solar activity.

The parameters to be measured in an S-16 type experiment are listed below.

1) Pitch-angle Distribution

The trapped radiation to be encountered by the Apollo earth-orbital missions over the South Atlantic will be highly directional, largely confined to a plane normal to the magnetic field. If it is assumed that the proton mirror-point density is inversely proportional to the effective atmospheric density, whose scale height, h, is constant, then we are able to show that the pitch angle distribution relative to the normal to the magnetic field is Gaussian with a variance given by

$$\sigma^2 = \frac{3}{4}\frac{h}{r_o}(2 + \cos^2 I),$$

where r_o is the dipolar radius, and I is the dip angle of magnetic field.

At an altitude of 140 n mi (260 km), where $h \approx 50$ km and $I \approx 42^\circ$ in the anomaly region,[2] the calculated standard deviation of the pitch angle distribution is $\sigma \approx 6.7^\circ$.

2) Directional Flux

In the South Atlantic anomaly the trapped particles are close to their mirror points. They are therefore, moving in, or at a small angle to, a plane which is perpendicular to the local direction of $\vec{B}$. Due to the density gradient of the atmosphere the directional flux in this plane is not isotropic. Fig.II-1 indicates how an east-west asymmetry arises. The asymmetry is a function of the momentum of the trapped particle and is given by

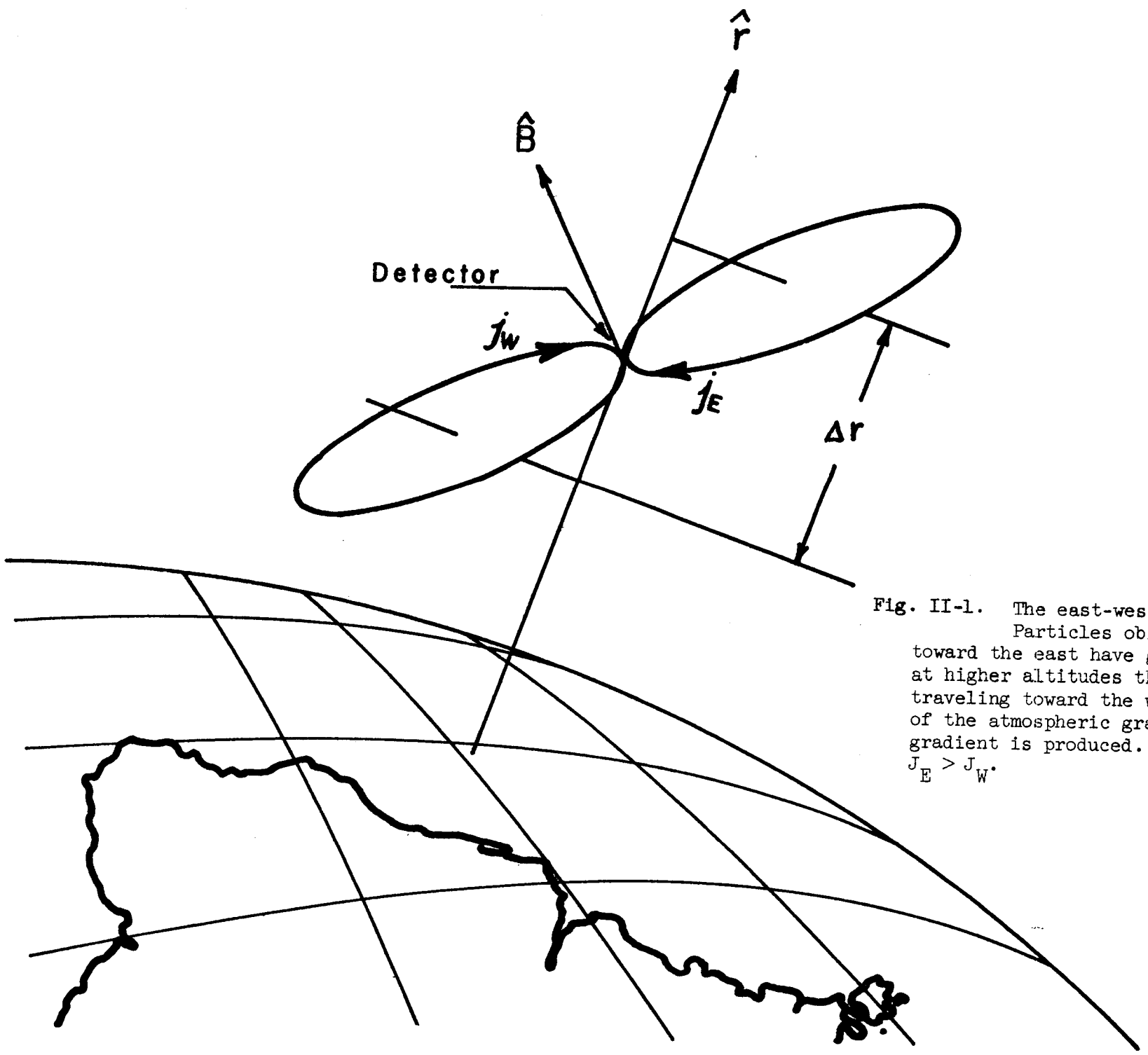

Fig. II-1. The east-west asymmetry. Particles observed traveling toward the east have guiding centers at higher altitudes than those traveling toward the west. Because of the atmospheric gradient, a flux gradient is produced. As a result $J_E > J_W$.

$$j_E/j_W = \exp\,[2ah^{-1}\cos I],$$

where a = pc/eB is the gyroradius of the trapped proton of momentum p, I is the dip angle of the B field, and h is the effective scale height of the atmosphere.[14]

The directional flux is measured on the sample of stopped protons in the energy range 50-160 MeV. Fig.II-2 gives the expected values of j_E/j_W for this energy range at an altitude of 140 n mi.

3) Proton Flux and Energy Spectrum

Fig.II-3 is a geographic iso-count contour representation of the omnidirectional proton flux as deduced from time-integrated emulsion flux measurements at 400 km altitude and Explorer XV data to obtain the shape of the contours. These data were taken during 1963-4, near solar minimum. Superimposed on the flux contours are Apollo orbits 4 through 10 which cross the South Atlantic during the first 24 hours. An integration of the proton flux over orbits 4-10 gives an estimate of the number of protons incident on the detector per day. At 400 km (215 n mi) the proton flux is $N = 1.4 \times 10^6$ cm^{-2} day^{-1} for an orbit of 28° inclination. A calculated result, which is consistent with our emulsion data, and that of Filz and Holeman,[10] is that the altitude variation of the proton flux is given by $N \propto [r_m \rho(r_m)]^{-1}$, where $\rho(r_m)$ is the density of the atmosphere at r_m, and r_m is the minimum mirror-point altitude. the COSPAR reference atmosphere (1961) has been used to evaluate the daily flux vs satellite altitude. The result is given in Fig. II-4.

4) Particle Mass Measurements

Present information indicates that an upper limit of ≈ 1 percent

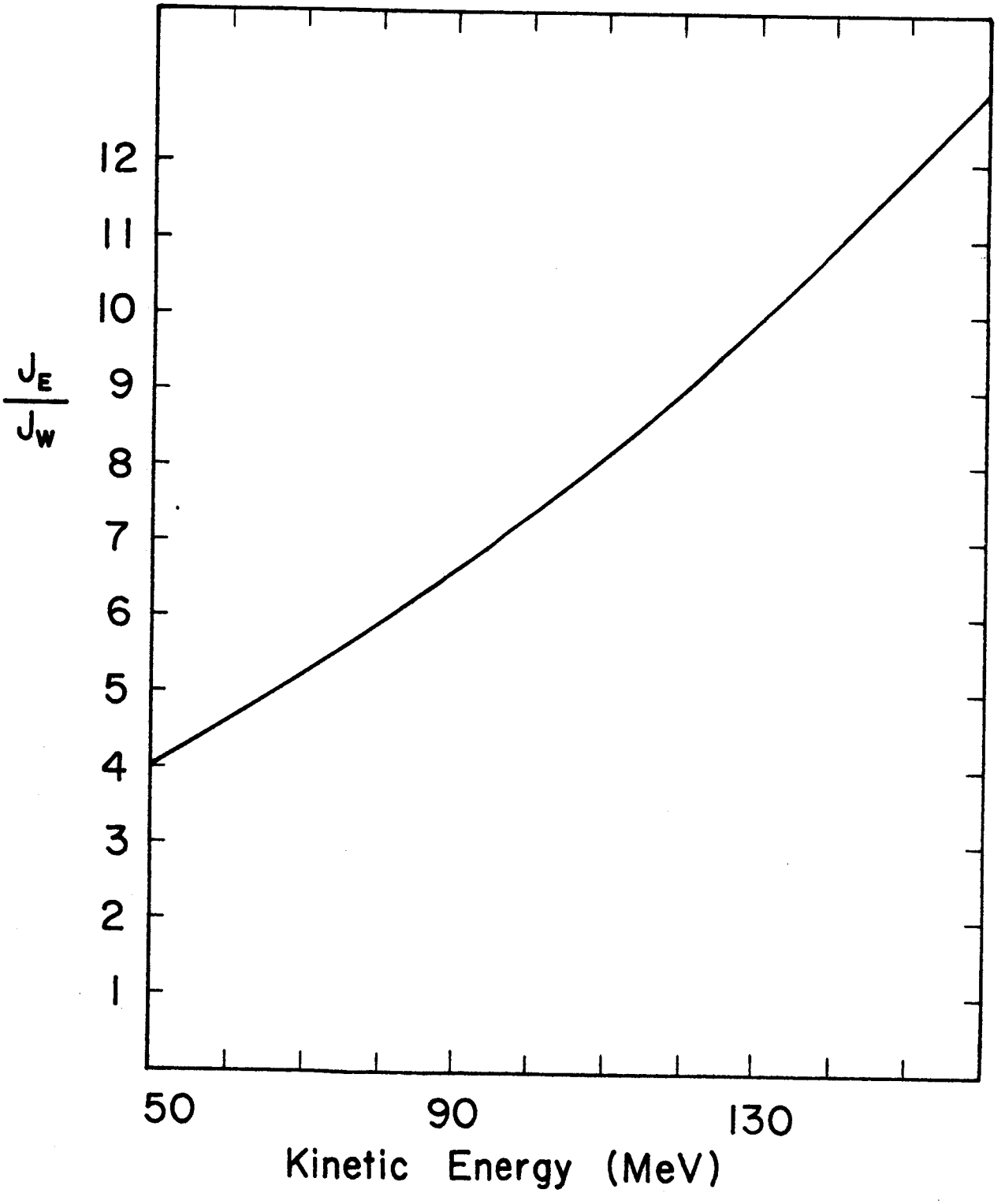

Fig. II-2. Ratio of east to west proton fluxes versus energy at 140 n mi

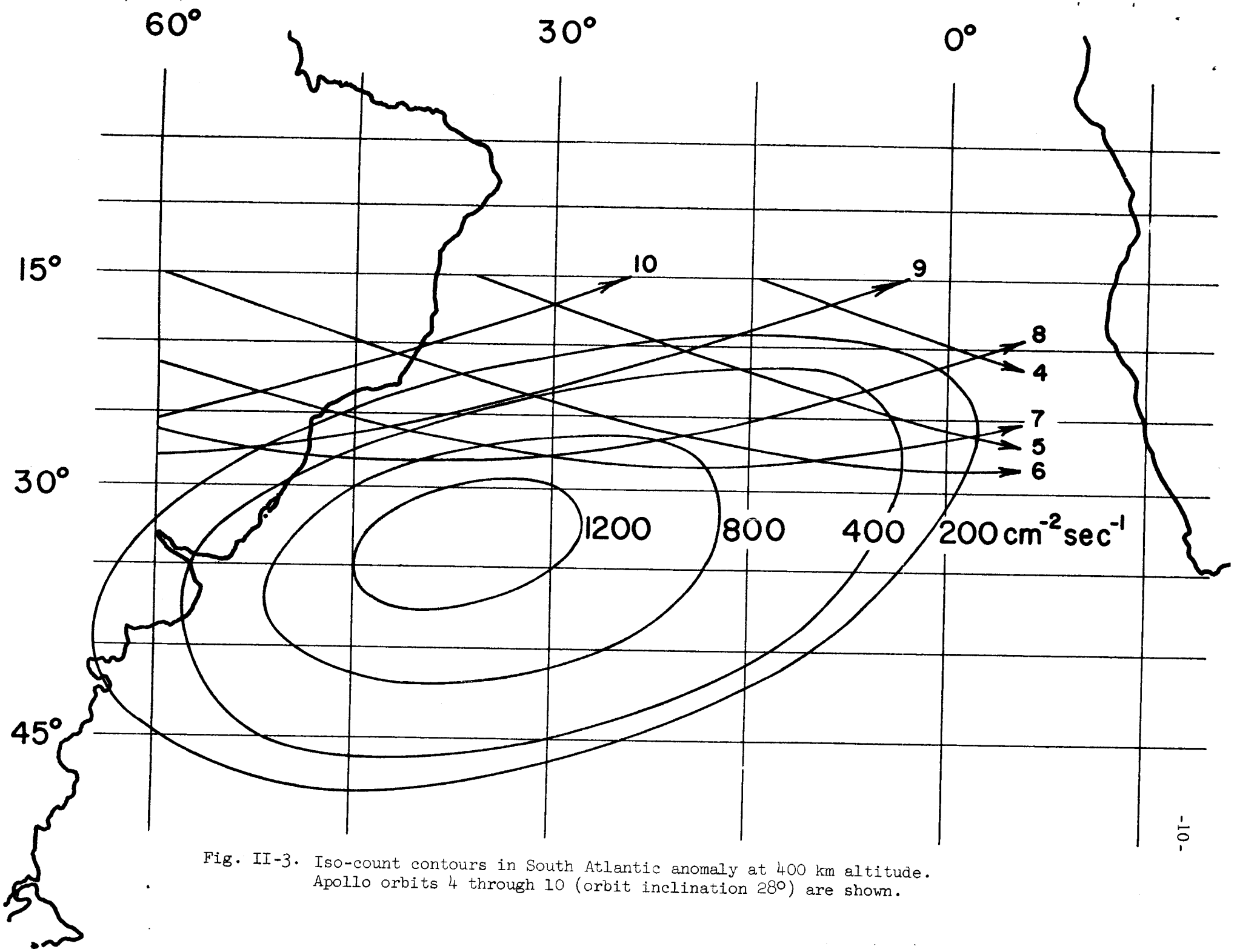

Fig. II-3. Iso-count contours in South Atlantic anomaly at 400 km altitude. Apollo orbits 4 through 10 (orbit inclination 28°) are shown.

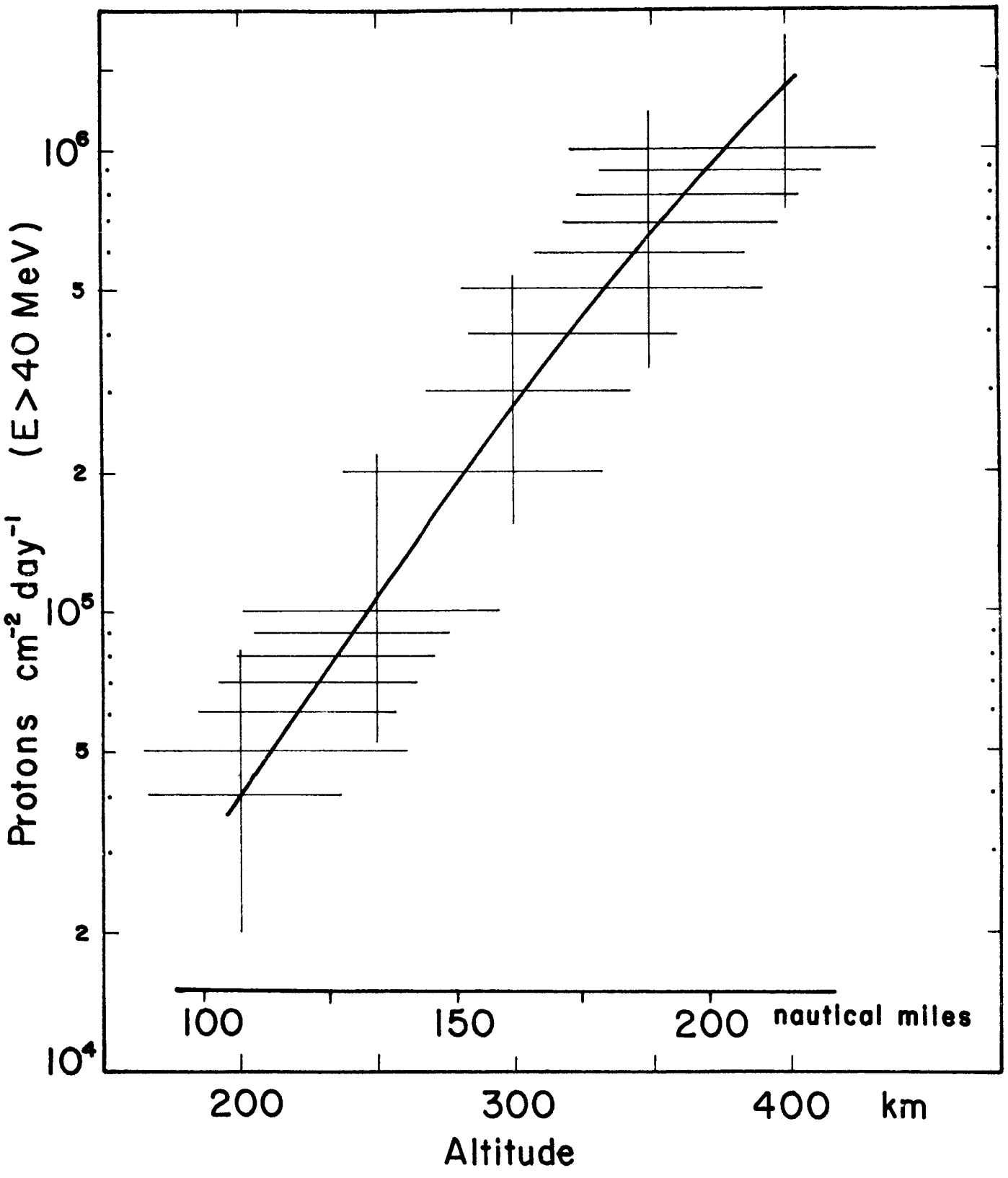

Fig. II-4. Estimated proton flux as a function of satellite altitude over anomaly.

of the nucleonic component of the trapped radiation may consist of particles heavier than protons. No alpha particles have been detected in the inner belt, although their presence is expected. A principal source of α-particles may be spallation products emitted from nuclear interactions between the trapped radiation and the atmosphere. If such is the case, the α-particle spectrum will have an evaporation-type energy spectrum where few α-particles greater than 40 MeV can be expected. A 40 MeV α-particle has a range of only 0.6 mm in emulsion (equal to a 10 MeV proton).

The basic research program we have described is to study systematically the interaction of the geomagnetically trapped protons with the atmosphere, and to observe and measure changes in the properties of the trapped radiation as a function of time during the solar-cycle period. From studies of this type, information will be gained about the sources (albedo neutrons -- galactic and solar, direct injection, etc.) and loss mechanisms (atmospheric, magnetic instabilities, etc.) of the particles which constitute the inner radiation belt. Such a study is appropriately carried out at low satellite altitudes in the South Atlantic anomaly.

Section II References

1. Heckman, H. H. and A. H. Armstrong, J. Geophys. Res. 67, 1255 (1962).

2. Heckman, H. H. and G. H. Nakano, J. Geophys. Res. 68, 2117 (1963).

3. Heckman, H. H. and G. H. Nakano, Space Research V, 329 (1965), and to be published.

4. Nakano, G. H. and H. H. Heckman, Phys. Rev. Letters 15, 806 (1968).

5. Blanchard, R. C. and W. N. Hess, J. Geophys. Res. 69, 3927 (1964).

6. Freden, S. C. and R. S. White, Phys. Rev. Letters, 2, 417 (1959).

7. Pizzella, G., C. E. McIlwain, and J. A. Van Allen, J. Geophys. Res. 67, 1235 (1962).

8. For a recent summary of counter results, see R. W. Fillius, J. Geophys. Res. 71, 97 (1966).

9. Filz, R. C. and E. Holeman, J. Geophys. Res. 70, 5807 (1965).

10. McIlwain, C. E., J. Geophys. Res. 66, 3681 (1961).

11. Valerio, J., J. Geophys. Res. 69, 4949 (1964).

12. Dragt, A. J., M. M. Austin and R. S. White, J. Geophys. Res. 71, 1293 (1966).

13. Hess, W. N. and J. Killeen, J. Geophys. Res. 71, 2799 (1966).

14. Lenchek, A. M. and S. F. Singer, J. Geophys. Res. 67, 4073 (1962).

III. ELECTRONIC COUNTER AND PARTICLE IDENTIFICATION

A. Description of Laboratory Prototype

The eight counter telescope that was constructed for this study appears in photographs, Figs. III-1-4. It consists of two physically separate units; the telescope housing containing eight solid state detectors, each with its separate preamplifier, and an electronic box containing the amplifiers, pulse shapers, analog-to-digital converters logic circuitry, and interface circuitry to an on-line PDP-5 digital computer.

A photograph of the detector assembly is shown in Fig. III-1. It consists of two 300 micron thick silicon diffused detectors that are coaxial with six 3 mm thick lithium drifted silicon detectors. Pulse amplitudes from all eight detectors are recorded for every particle event.

The detector assembly is mounted in a plastic fluor (~ 1 cm thick) which is cemented to the face of an RCA 2067 phototube. Figure III-2 shows the detector and fluor assemblies and the pre-amplifier electronics. The fluor assembly containing the detector fits inside the circular electronic boards and the entire system is enclosed in a metal housing.

A top view of the other unit which comprises the bulk of the electronic circuitry is shown in Fig. III-3. The circuit cards, which are viewed end-on, will be subsequently described. They are the following: eight amplifier-converter cards, one discriminator card, one input control card, one output control card, four dual binary cards, one gated oscillator card, and a computer interface card; a total of 17 printed circuit boards. Also shown are the converters that supply

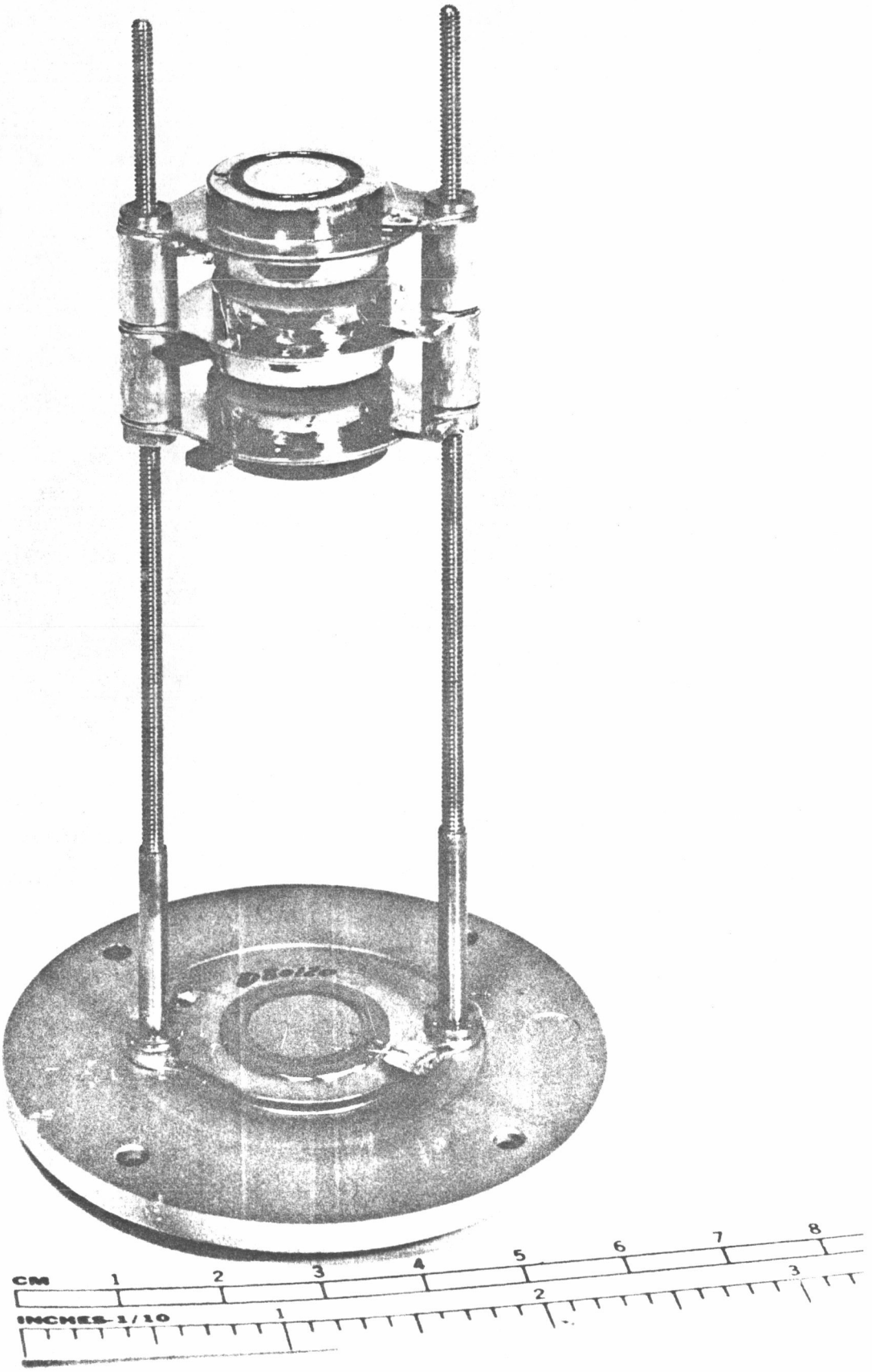

Fig. III-1. Detector assembly

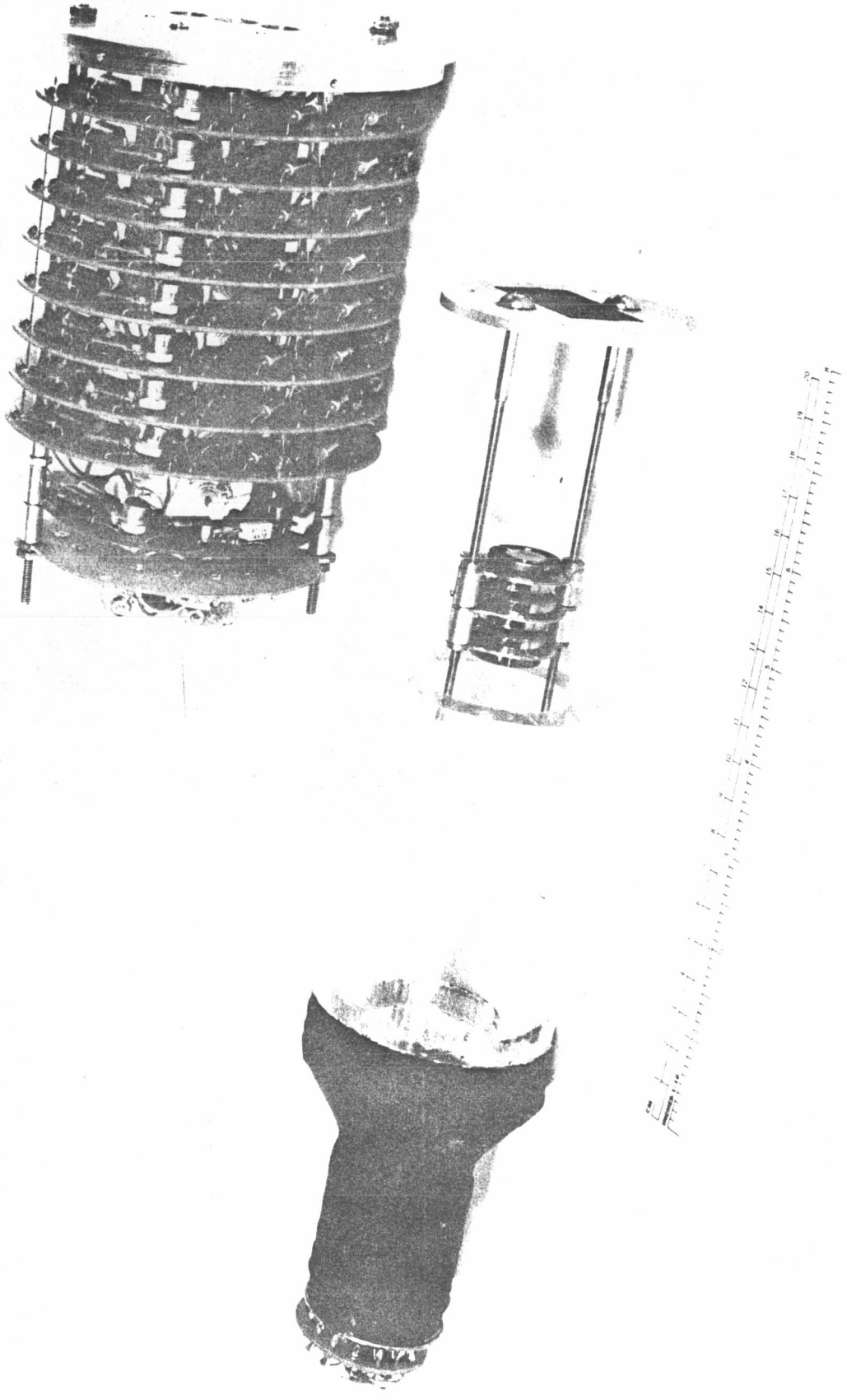

Fig. III-2. Detector and fluor assemblies and pre-amplifier electronics

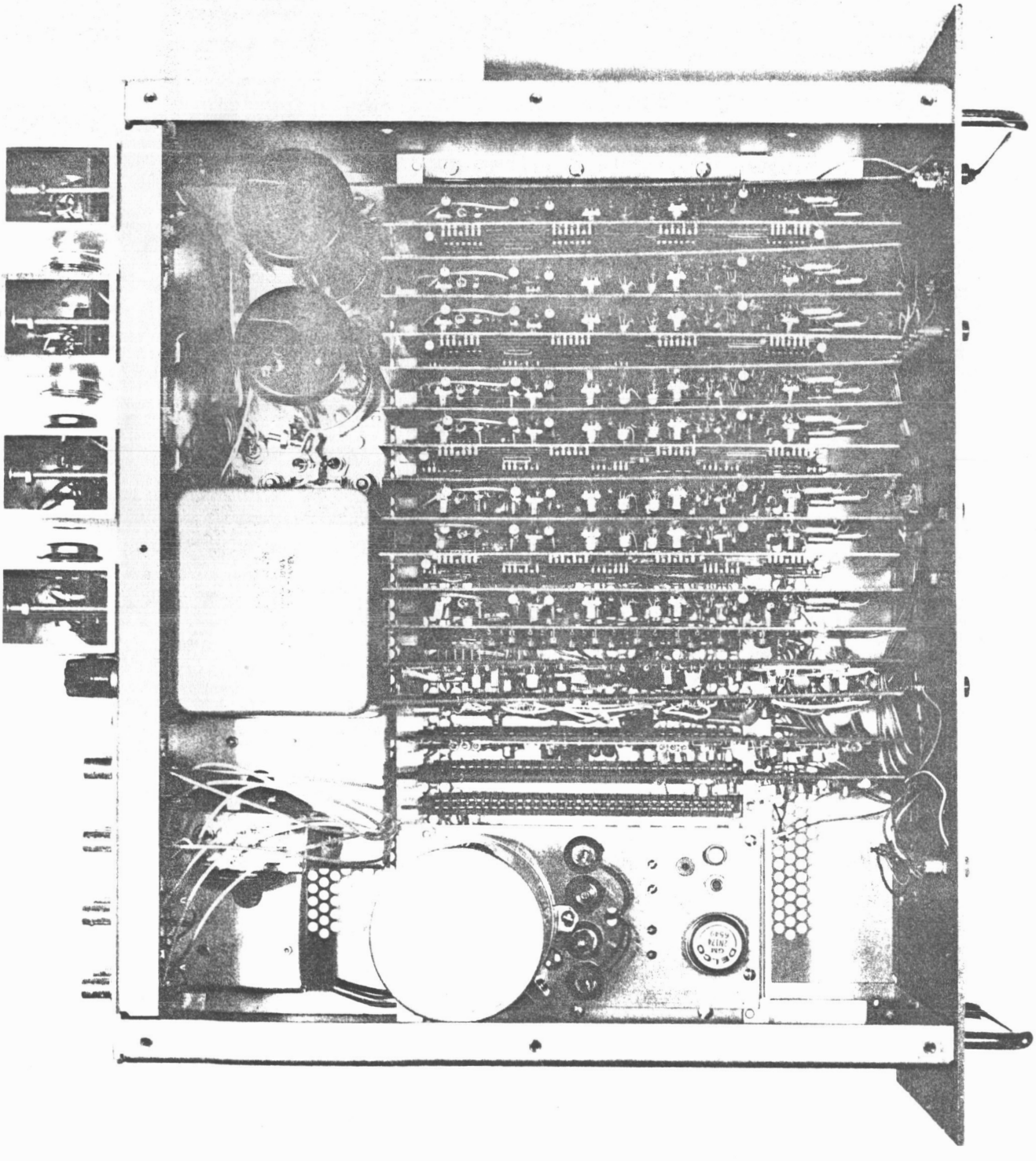

Fig. III-3. View of the main body of electronic circuitry.

voltages required for the various circuits.

Figure III-4 is a front view of the electronics box. Various test points are available for monitoring strategic points in the circuitry.

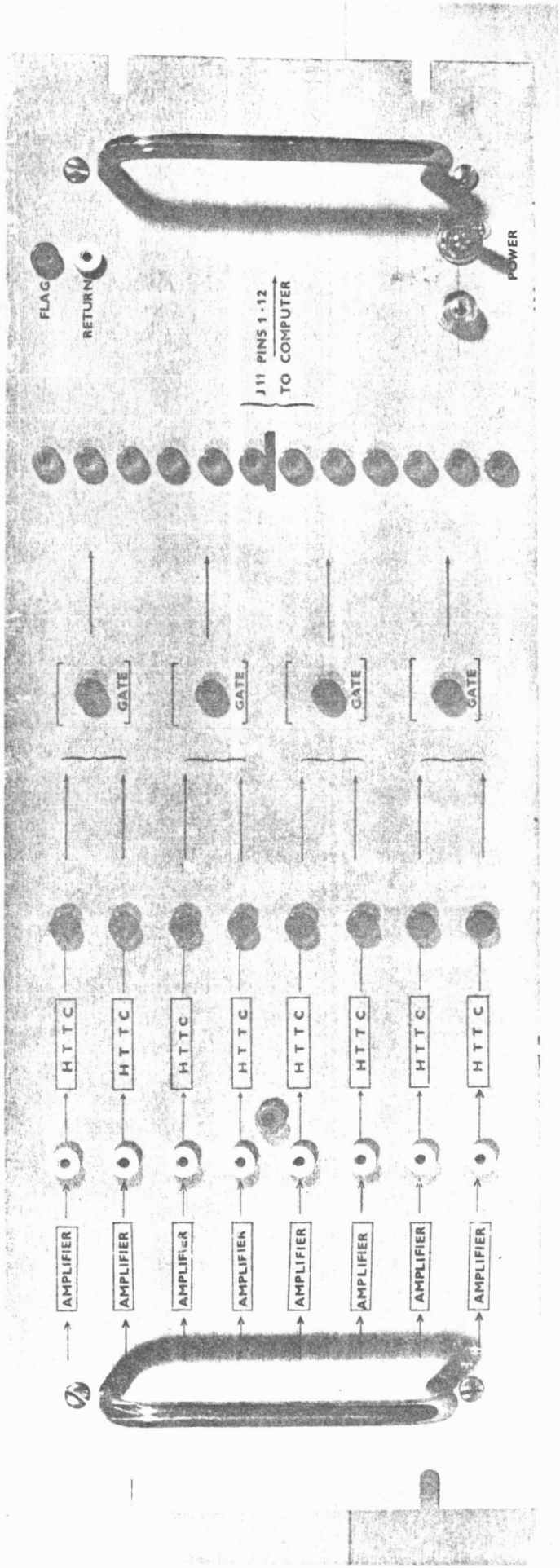

Fig. III-4. Front view of electronics cabinet

B. Theory of Operation

The system block diagram (Fig. III-5) illustrates the basic electronic operation of the eight-counter telescope. Essentially, for each event, all signals generated by passage of a particle through the detectors are amplified by a charge-sensitive pre-amplifier before they enter the pulse shaping (0.2 μs RC) amplifier. If the event is acceptable (an acceptable event will be defined later), the signals are passed by a linear gate into an analog-to-digital converter. The A-D conversion is accomplished by use of a height-to-time converter of the Wilkinson run-down type. Digital pulse height information from each detector is then stored in a 6 bit binary string before being read out into the PDP-5 computer. The computer CRT is used for line display and information obtained for each event is ultimately stored on IBM compatible magnetic tape for further processing with the LRL CDC 6600 data processor.

The system block diagram also indicates points at which test pulses are injected to calibrate the electronic response of the eight-counter telescope. A Berkeley tail pulser is used for this purpose. A dial setting of 0.1 corresponds to a 10 MeV signal. The electronics handles up to 10 MeV signals for the thin detectors and up to 100 MeV signals for the thick detectors. The photomultiplier also has a test input to allow system checks of its circuits.

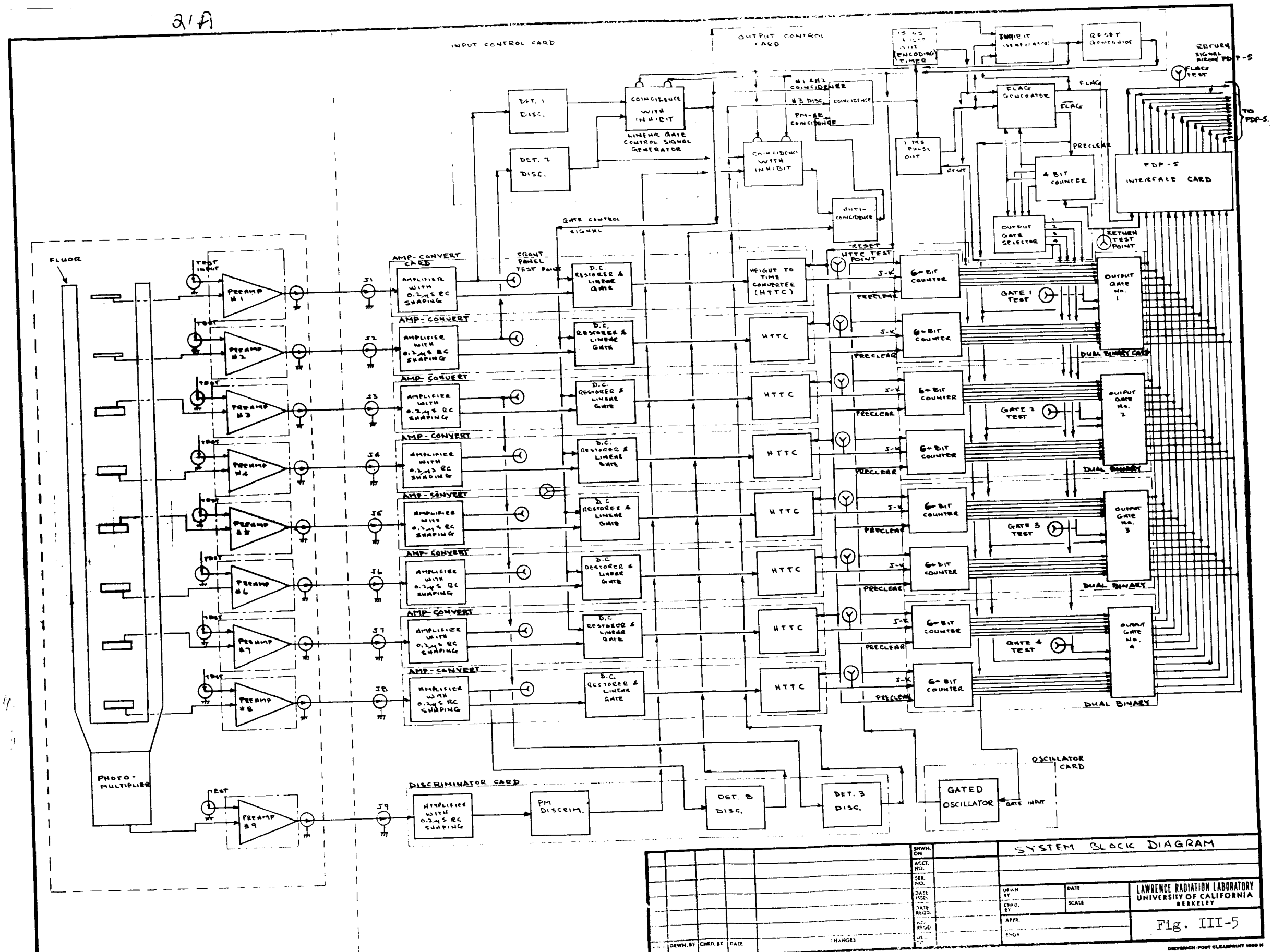
INPUT CONTROL CARD
OUTPUT CONTROL CARD
FLUOR
PHOTO-MULTIPLIER
TEST INPUT
PREAMP #1
PREAMP #2
PREAMP #3
PREAMP #4
PREAMP #5
PREAMP #6
PREAMP #7
PREAMP #8
PREAMP #9
J1
J2
J3
J4
J5
J6
J7
J8
J9
AMP-CONVERT CARD
AMPLIFIER WITH 0.2μs RC SHAPING
FRONT PANEL TEST POINT
DET. 1 DISC.
DET. 2 DISC.
COINCIDENCE WITH INHIBIT
LINEAR GATE CONTROL SIGNAL GENERATOR
GATE CONTROL SIGNAL
#1 & #2 COINCIDENCE
#3 DISC.
PM-#6 COINCIDENCE
ANTI-COINCIDENCE
1 MS PULSE OUT
RESET
D.C. RESTORER & LINEAR GATE
HEIGHT TO TIME CONVERTER (HTTC)
HTTC TEST POINT
J-K'
PRECLEAR
6-BIT COUNTER
4 BIT COUNTER
OUTPUT GATE SELECTOR
FLAG GENERATOR
FLAG
PDP-5 INTERFACE CARD
RETURN SIGNAL FROM PDP-5
FLAG TEST
TO PDP-5
RETURN TEST POINT
GATE 1 TEST
GATE 2 TEST
GATE 3 TEST
GATE 4 TEST
OUTPUT GATE NO. 1
OUTPUT GATE NO. 2
OUTPUT GATE NO. 3
OUTPUT GATE NO. 4
DUAL BINARY
DISCRIMINATOR CARD
PM DISCRIM.
DET. 8 DISC.
DET. 3 DISC.
GATED OSCILLATOR
GATE INPUT
OSCILLATOR CARD
SYSTEM BLOCK DIAGRAM
LAWRENCE RADIATION LABORATORY
UNIVERSITY OF CALIFORNIA
BERKELEY
Fig. III-5

C. Circuit Design

1. Preamplifiers

The preamplifiers, which are of standard cascode design, are shown in the detector preamplifier (Fig. III-6) and the phototube preamplifier (Fig. III-7) drawings.

2. Amplifiers and Converters

Operation of the amplifier and converter circuits is shown in the block diagram of Fig. III-8. Signals from the preamplifiers are processed through linear amplifiers having 0.2 μs RC pulse shaping. The dc level of these signals is clamped using a dc restorer before passing through a linear gate to the height-to-time converter. The converter transforms the pulse to a time width that is proportional to the amplitude of the pulse. A maximum signal amplitude of 8 volts corresponds to a maximum width of 12 μsec. The HTTC is a simplified version of the Wilkinson circuit used in the Berkeley ADC.

3. Dual Binary Output

The time pulse from the HTTC opens the input gate to the 6 bit counter and simultaneously triggers a 15 μs pulse in the encoding timer which is used to turn on the gated oscillator. This results in encoding the detector pulse into one of 64 possible levels. The encoded signals are retained in 6 bit counters until either read out is completed or the expiration of a 1 ms retaining pulse occurs, whichever takes place first. These operations are indicated on the binary output block diagram (Fig. III-9).

4. Input Control Board

Selection of acceptable pulses to be analyzed is determined by the logic included in the input and output control circuits. The

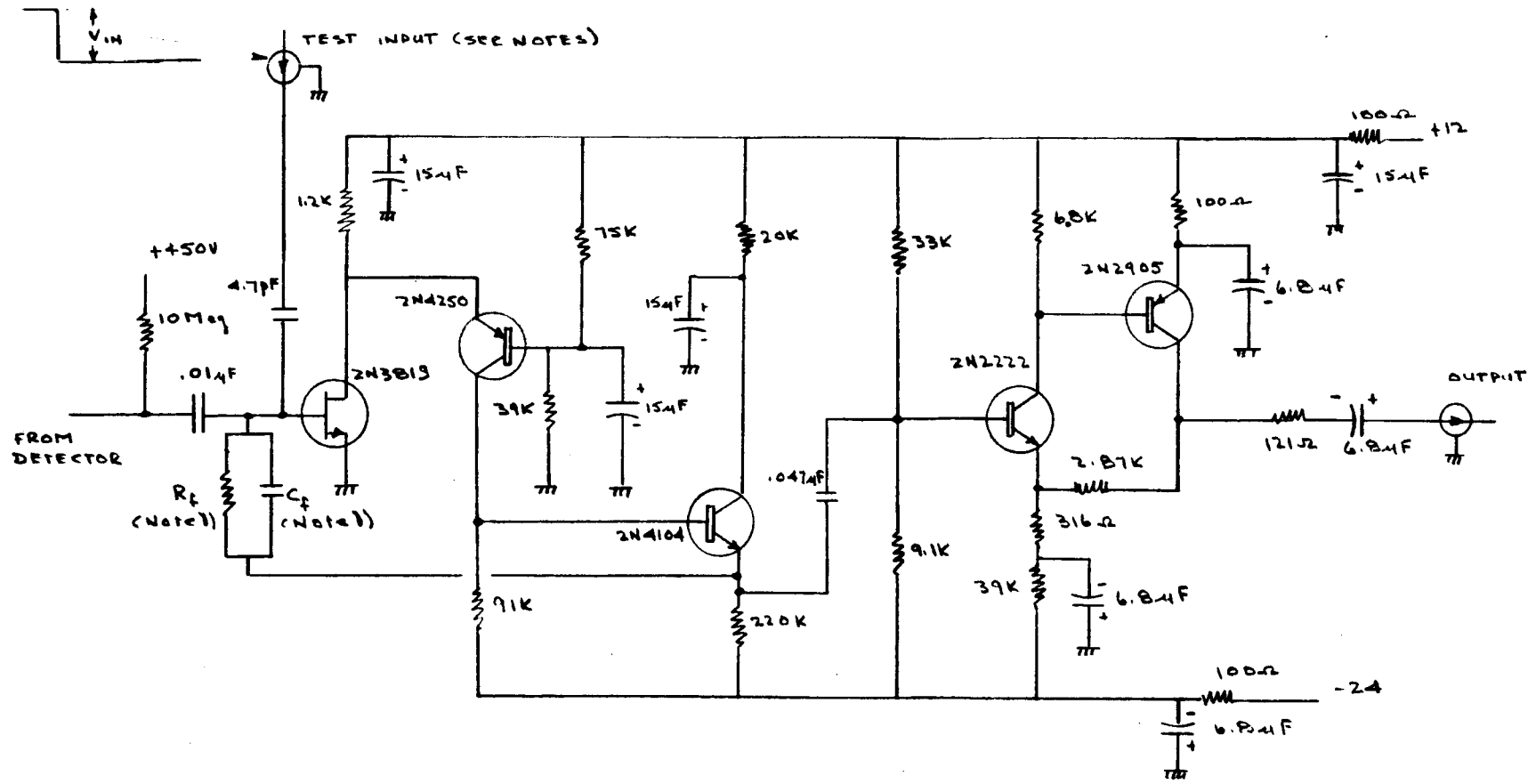

OUTPUTS CORRESPONDING TO THE V_{IN} TEST LEVELS

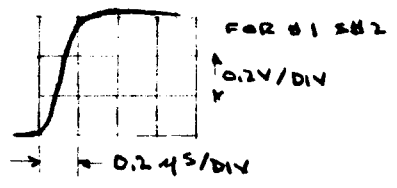

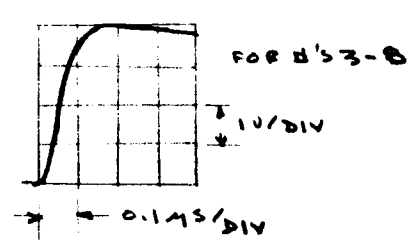

NOTES

1) R_f & C1 ON DETECTORS 1 & 2 HAVE VALUES OF 1Meg and 2.2pF, WHILE ON THE REMAINING DETECTORS HAVE VALUES OF 1Meg & 4.7pF
2) V_{IN} FOR #1 & #2 SHOULD BE 0.094BV TO CORRESPOND TO A 10 MEV SIGNAL, WHILE ON #'S 3-8 V_{IN} SHOULD BE 0.948V TO CORRESPOND TO A 100 MEV SIGNAL

					SHWN. ON		ENGINEERING SKETCH —
					ACCT. NO.		DETECTOR PREAMPLIFIER SCHEMATIC
					SER. NO.		
					DATE ISSD.	DRWN. BY	DATE
					DATE RETD.	CHKD. BY	SCALE
					INT. REQ'D.	APPR.	LAWRENCE RADIATION LABORATORY UNIVERSITY OF CALIFORNIA BERKELEY
CHG	DRWN. BY	CHKD. BY	DATE	CHANGES	DET. TO	SHT. #	Fig. III-6

RL-398-1

FOLDOUT FRAME 1

FOLDOUT FRAME 2

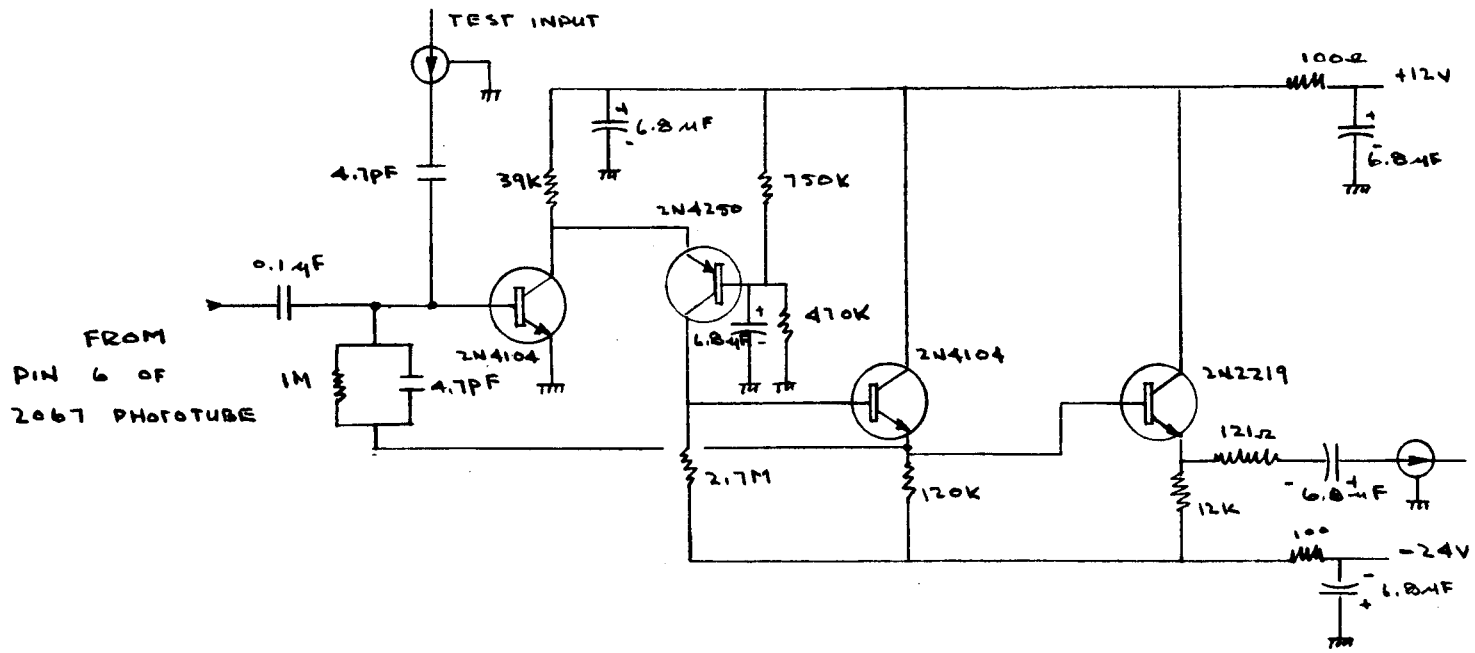

					SHWN. ON		ENGINEERING SKETCH —
					ACCT. NO.		PHOTOTUBE PREAMPLIFIER
					SER. NO.		
					DATE ISSD.	DRWN. BY / DATE	LAWRENCE RADIATION LABORATORY UNIVERSITY OF CALIFORNIA BERKELEY
					DATE RECD	CHKD. BY / SCALE	
					NO. SHTS.	APPR.	Fig. III-7
CNG.	DRWN. BY	CHKD. BY	DATE	CHANGES	DLG. NO.	ENGR.	

RL-398-1

DIETZGEN POSTCLEANPRINT 1000 H

FOLDOUT FRAME 1

FOLDOUT FRAME 2

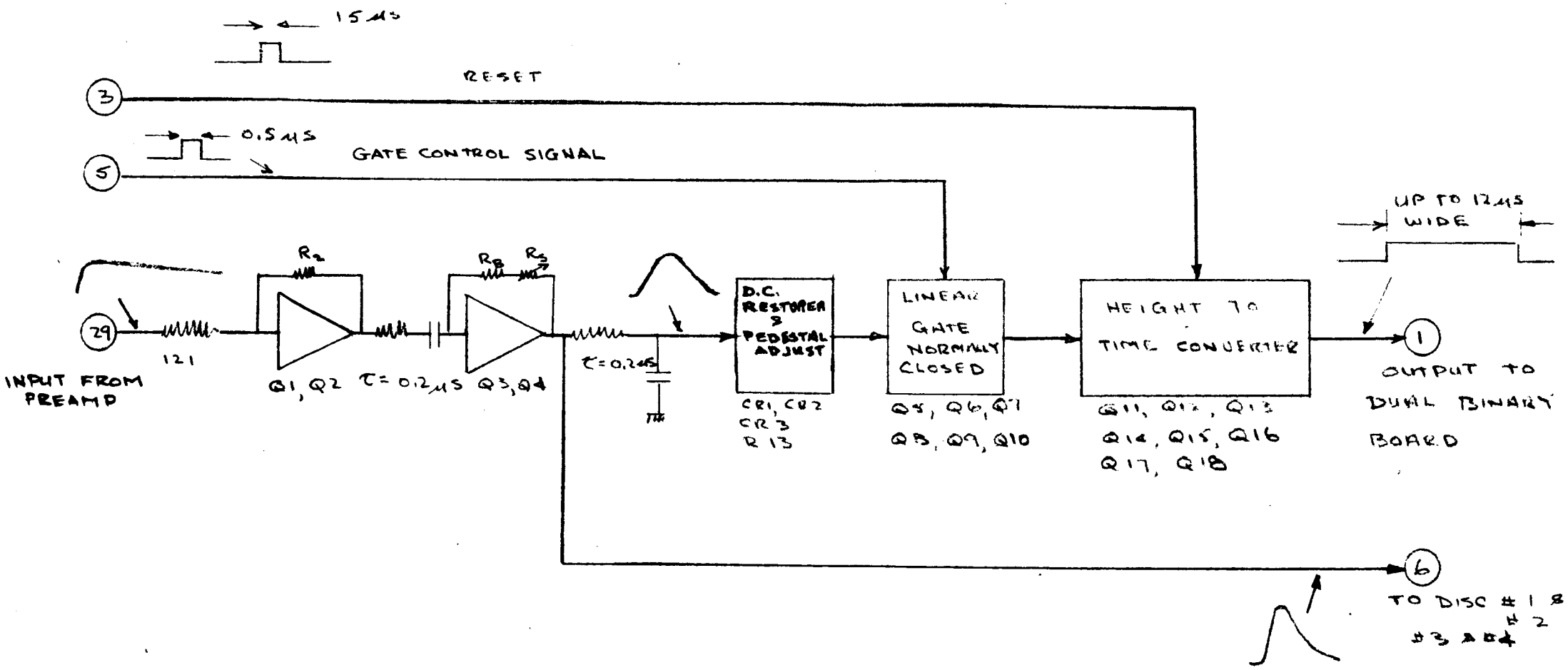

CHG.	DRWN. BY	CHKD. BY	DATE	CHANGES

SHWN. ON	
SHWN. ON	
ACCT. NO.	
SER. NO.	
DATE ISSD.	
DATE REQD.	
NO. REQD	
DEL. TO	

BLOCK DIAGRAM OF AMPLIFIER-CONVERTER BOARD

DRWN. BY	DATE
CHKD. BY	SCALE
APPR.	
ENGR	

LAWRENCE RADIATION LABORATORY
UNIVERSITY OF CALIFORNIA
BERKELEY

Fig. III-8

RL-2009-1 (REV. 2-66)

FOLDOUT FRAME 1

FOLDOUT FRAME 2

DIETZGEN POSTCLEARPRINT 1000 H

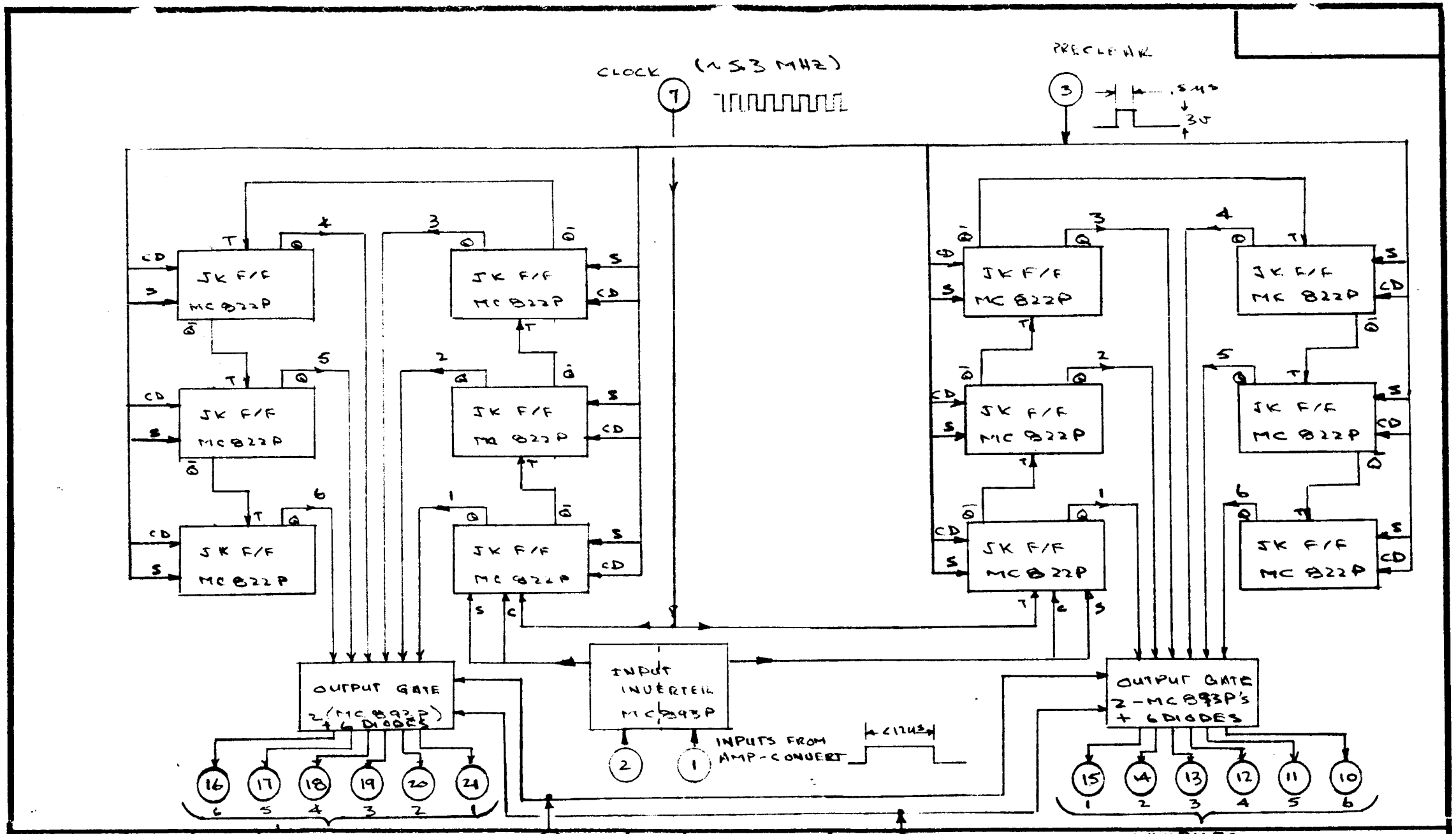

				OUTPUTS FLAG (28) VARIABLE	SHWN. ON		(27) SELECTOR OUTPUTS VARIABLE	
					SHWN. ON			
					ACCT. NO.		DUAL BINARY OUTPUT BLOCK DIAGRAM	
					SER. NO.			
					DATE ISSD.		DRWN. BY / DATE	LAWRENCE RADIATION LABORATORY UNIVERSITY OF CALIFORNIA BERKELEY
					DATE REQD.		CHKD. BY / SCALE	
					NO. REQD.		APPR.	Fig. III-9
CHG.	DRWN. BY	CHKD. BY	DATE	CHANGES	DEL. TO		ENGR.	

RL-2009-1 (REV. 2-66)

FOLDOUT FRAME 1

FOLDOUT FRAME 2

DIETERICH-POST CLEARPRINT 1000 H

block diagram for the input control board is shown in Fig. III-10. Amplifier outputs from the first two detectors are converted into two 50 ns time pulses which are connected in coincidence. If no inhibit pulse from the 15 μs encoding signal or the 1 ms read-out retaining signal is present, an input control signal, which is a 0.5 μs pulse, is generated. This signal opens the linear gates and also goes to the output control board. The 50 ns pulse from discriminator 2 is applied to a coincident circuit on the output control board which also is connected to the phototube discriminator output.

5. Output Control Board

Figure III-11 is a block diagram of the output control board. An anticoincidence pulse from the phototube is generated in ML1 unless a signal is simultaneously produced in the eighth detector. If a signal is simultaneously produced in the first 3 detectors and no anticoincidence pulse is generated, the encoding begins and the event is considered acceptable. In this event the 1 ms read-out signal is also generated. In the event that the signal is not acceptable in the previously stated sense, a 15 μs pulse resets the flip-flops and the height-to-time converter circuits. This gate is triggered at the end of the 0.5 μs input control signal. When the encoding is completed at the end of 15 μs a flag signal is sent to the computer to indicate the readiness for read-out of the binaries. The read-out is accomplished in increments of 12 bits or one pair of 6 bit counters at a time. At the end of the first read-out, a complete signal from the computer advances the read-out, one step at a time, as determined by the state of the 2 bit counter on the output control card. Thus, four such read cycles are required to read out each acceptable event.

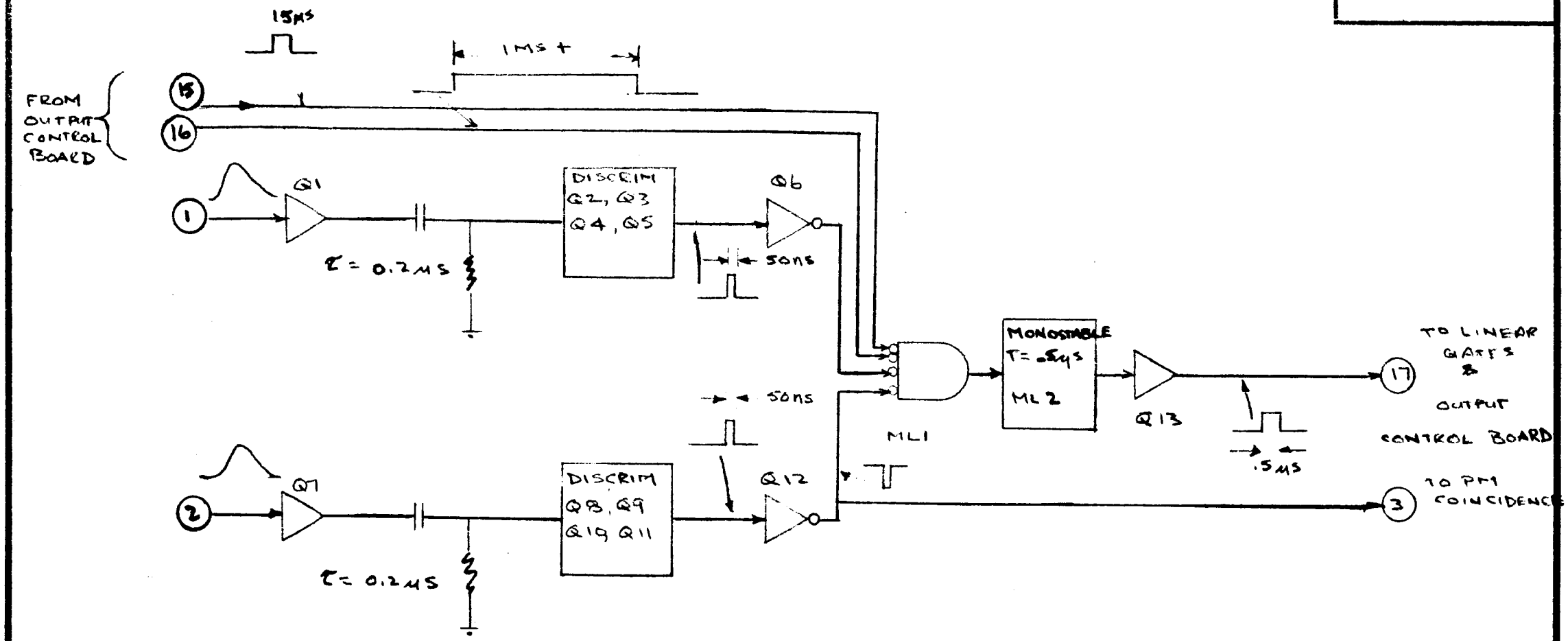

CHG.	DRWN. BY	CHKD. BY	DATE	CHANGES

SHWN. ON	
SHWN. ON	
ACCT. NO.	
SER. NO.	
DATE ISSD.	
DATE REQ'D.	
NO. REQD.	
DEL. TO	

BLOCK DIAGRAM FOR
INPUT CONTROL BOARD

DRWN. BY	DATE
CHKD. BY	SCALE
APPR.	
ENGR.	

LAWRENCE RADIATION LABORATORY
UNIVERSITY OF CALIFORNIA
BERKELEY

Fig. III-10

RL-2009-1 (REV. 2-66)

DIETERICH POST CLEARPRINT 1000 H

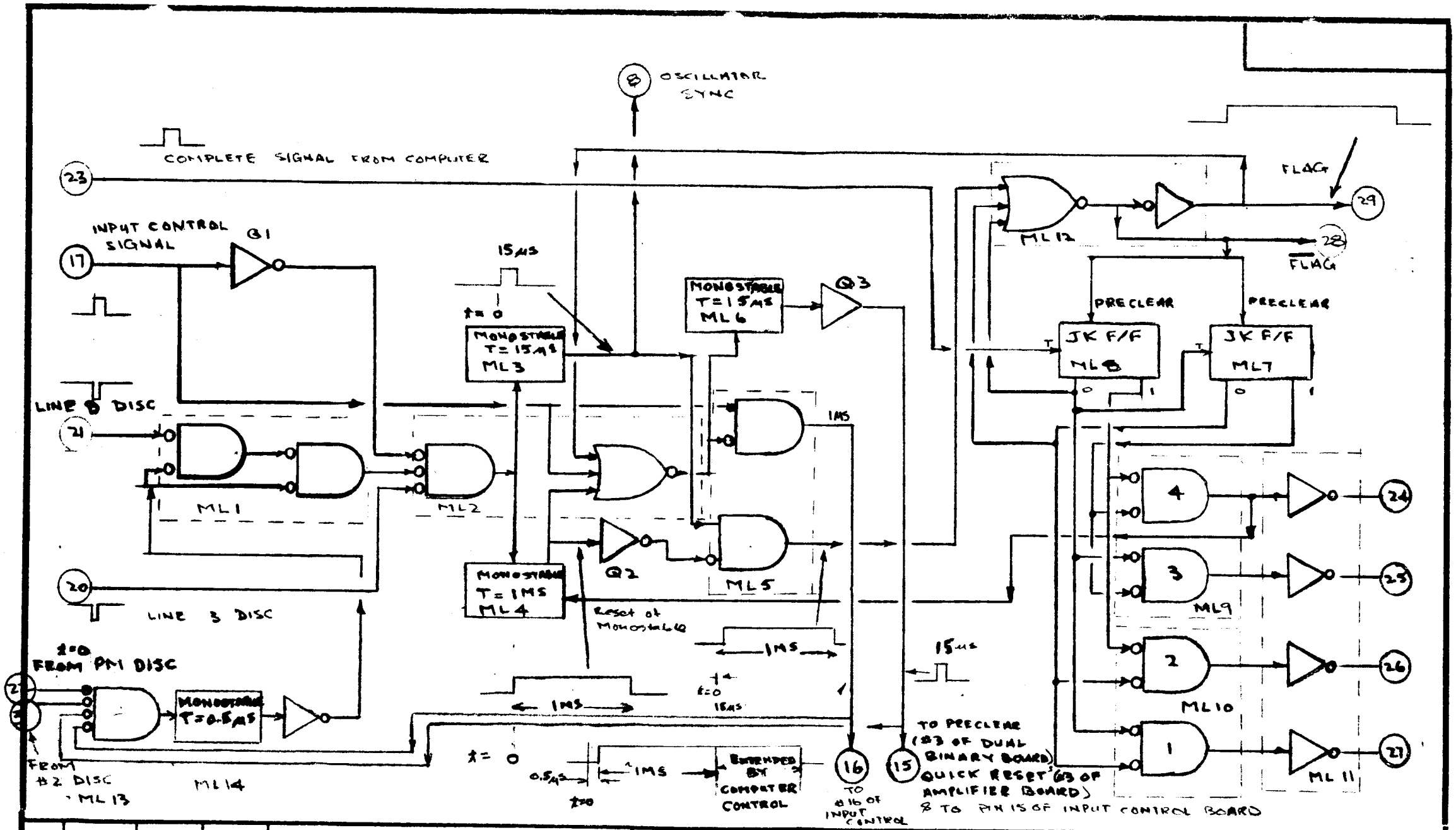

CHG.	DRWN BY	CHKD. BY	DATE	CHANGES

SHWN. ON	
SHWN. ON	
ACCT. NO.	
SER. NO.	
DATE ISSD.	
DATE REQD.	
NO. REQD.	
DEI 10	

BLOCK DIAGRAM OF OUTPUT CONTROL BOARD

DRWN. BY	DATE	LAWRENCE RADIATION LABORATORY UNIVERSITY OF CALIFORNIA BERKELEY
CHKD. BY	SCALE	
APPR.		Fig. III-11
ENGR		

RL-2009-1 (REV. 2-66)

During encoding, read-out and reset times, the signals from the first two discriminators are inhibited and hence the linear gates remain closed. This inhibit signal also prevents anticoincidence signals from being generated. All the digital signals to and from the converter pass through the interface card. This allows the conversion of the logic levels of the converter (+3,0) to the logic levels of the storage device and vice versa.

6. Subsequent Development

As no restrictions were placed on the size or power consumption of this unit, no extensive effort was expended on keeping the size small or the power consumption low. Reduction in size could be obtained by use of linear integrated circuits for some of the amplifier stages. This may cost some in power, however (e.g. the Sylvania SA 20 Video Amplifier has an 18 ma standing current drain while each discrete amplifier used in the design has about 5 ma).

While low power RTL μ Logic was used in design of the 6 bit counters MOST logic circuits would reduce both the power and size requirements of these 6 bit counters. Further, normal medium power RTL was used in the design of the output control card. This could readily be converted to low power RTL, or with some redesign to MOST logic.

D. Analysis of Pulse Height Data

The recorded data consists of a set of eight pulse heights for each event. These pulse heights tell us the energy which was deposited in each counter. This energy has an uncertainty which is the corresponding bin width. The analysis consists of asking what is the probability a given particle would produce the observed set of pulses. The energy loss distribution produced when a particle passes through matter is well known. For thin absorbers it is the Vavilov distribution.[1] For thick absorbers and large energy losses the distribution has been studied recently by Tschalär.[2,3] Experimental verification in the Vavilov region was done by Maccabee.[4] We have produced computer codes to evaluate these distributions. The important fact here is that the resultant distribution depends on a particle's mass, charge and energy in addition to the thickness of the absorber through which it passes.

The probability a certain particle caused an event is the product of the probabilities of producing the observed pulse in each counter. The probability a particle produced the pulse in a counter is the integral of the energy loss distribution function over the bin width of that counter. The probability is then maximized with respect to the incoming particle's energy. Thus, analysis by this method provides us with a probability that each particle of energy E caused the event.

Monte Carlo calculations with approximately the above counter configuration have shown particle identification to be certain to one part in 10^4 over the following energy ranges.

	Lower Limit	Upper Limit
He^4	50	265
He^3	45	235
T	20	105
D	20	90
P	15	65
π	7	29

The energy resolution was seen to be better than 1 percent.

E. Performance of Laboratory Prototype

Operational checks of the counter are in progress and our results on the performance of the counter are preliminary. We have taken data with the prototype counter using a momentum analyzed beam of protons at the LRL 184" cyclotron. Several energies were used and nuclear emulsions were exposed to calibrate the energy of the beam. Thus we shall use the known beam to calibrate the counter. Calibration consists of accurately defining the counter thickness and also the active layer thickness of each counter.

An option in the program which records the pulses for each event provides us with an oscilloscope display of the energy distribution in each counter. These displays were photographed at various energy settings. The energy distributions in counters 1-4 for incoming protons at 25 and 37.7 MeV are shown in Fig. III-12. There are several features of interest in these distributions.

1. Counters 1 and 2 clearly show the counters' sensitivity decrease in dE/dx with energy
2. The shift of the energy peak from counter 3 to counter 4 as the energy increases is shown.

The width of the distribution in the figure is due mainly to a 3-5 percent spread in the incoming proton energies. These events are being used in conjunction with the emulsion data to determine the dead layer thicknesses and thus calibrate the thick counters. The calibration process consists of finding the active area thickness which give consistent results for all the various energies used in the exposure.

The two leading thin counters have been accurately measured and

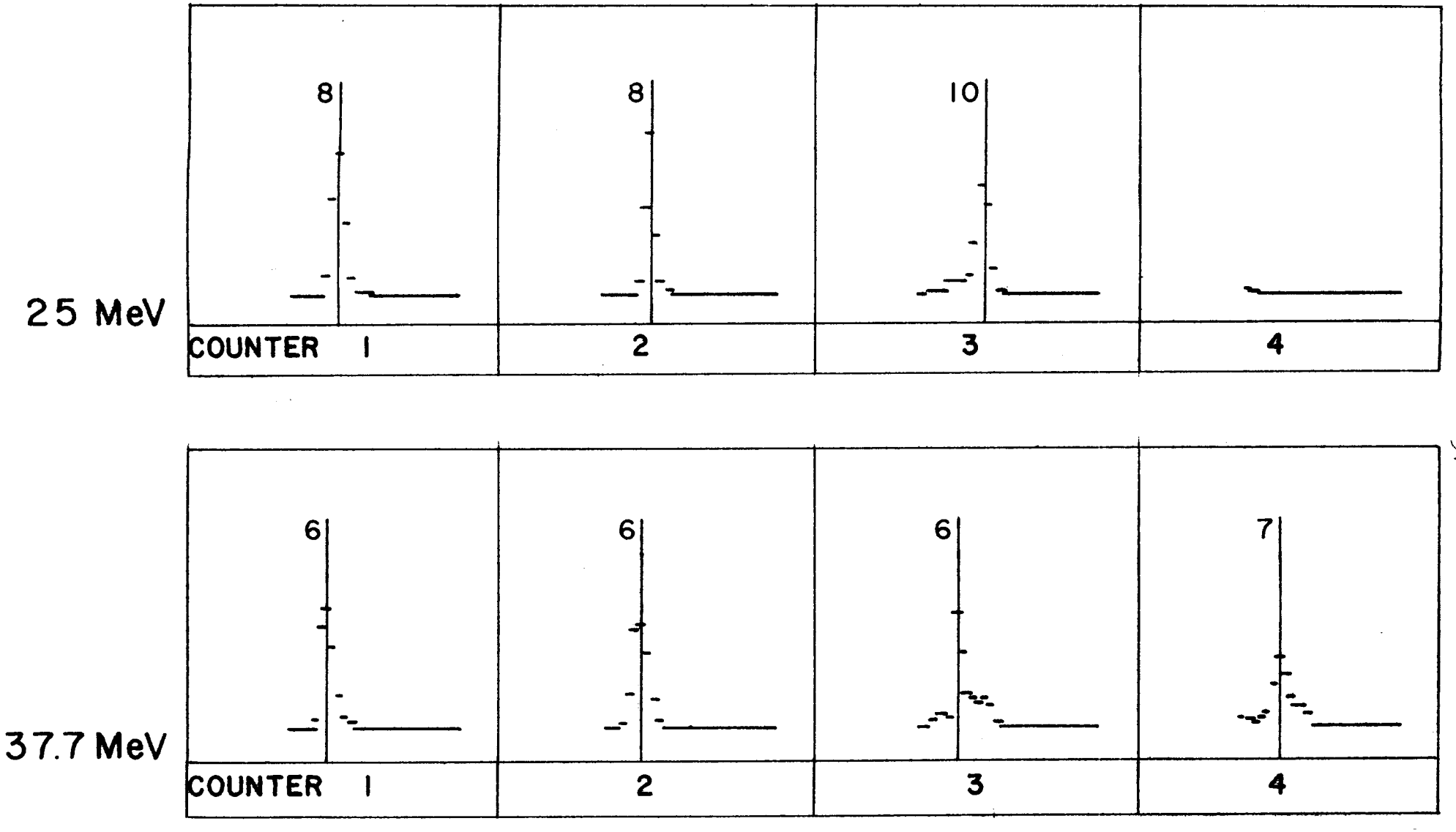

Fig. III-12. Pulse Height Distributions for counters 1-4 exposed to input proton average energies 25 and 37.7 MeV. Note shift in first two counters due to decreasing dE/dx and also penetration to counter 4 by the higher energies. The width of the peaks is mainly due to the spread of energies present in the proton beam. The channel in which the maximum number of counts were recorded is indicated.

found to be 323 ± 3μ thick. The corresponding energy distribution data tapes were generated and used in the program which calculates the earlier mentioned probability or Likelihood Function. Using these two thin counters alone energies could be determined to the order of 10 percent. It is clear even at this early stage in the analysis that the energy determination will be quite accurate when all eight counters are used. In early May we have 184" cyclotron time reserved to expose to particles other than protons. A further report will present the results of this test.

Section III References

1. P. V. Vavilov, Zh. Exper. Teor. Fiz. 32, 320 (1957).
Transl., JETP. 5, 749 (1957).

2. C. Tschalär, Rutherford High Energy Laboratory Report, RHEL/R146.

3. C. Tschalär, Rutherford High Energy Laboratory Report, RHEL/R153.

4. Howard David Maccabee, UCRL-16931.

IV. REQUIREMENTS FOR A FLIGHT EXPERIMENT, AAP MISSION

A. Geometry

The trapped radiation in the South Atlantic anomaly is localized in a plane, the normal of which is the earth's magnetic field vector. As illustrated in Fig. II-1, the directional flux of energetic protons is asymmetric in the mirror plane. One of the objectives of a low-altitude, earth-orbit experiment would be to measure this particle (east-west) asymmetry.

An obvious and direct method for measuring the east-west asymmetry is through the use of one or two pairs of particle detectors. The counters would be of the particle identifier type, but mass identification would be required on a single pair only. The capability for mass measurements should be maintained, however, for redundancy and back-up when long duration missions are to be considered.

Figure IV-1 illustrates a typical experimental geometry. Shown are two pairs of counters, diametrically opposed, with a 90° separation between the pairs. The counters are located such that when all are in the mirror plane of particles, the narrow axis of the entrance slit is along $\vec{B}$.

To deduce the spatial orientation of the counters during periods of data acquisition will require 3-coordinate magnetometer data, indicated by the field components B_x, B_y, and B_z, Fig. IV-1, and the geographic location of the spacecraft.

B. Orientation

Because of their narrow pitch angle distribution, trapped particles will be detected only when the x and/or y axes are $\lesssim 30^{\circ}$ from the particles' mirror plane. The detectors therefore need be sensitive to

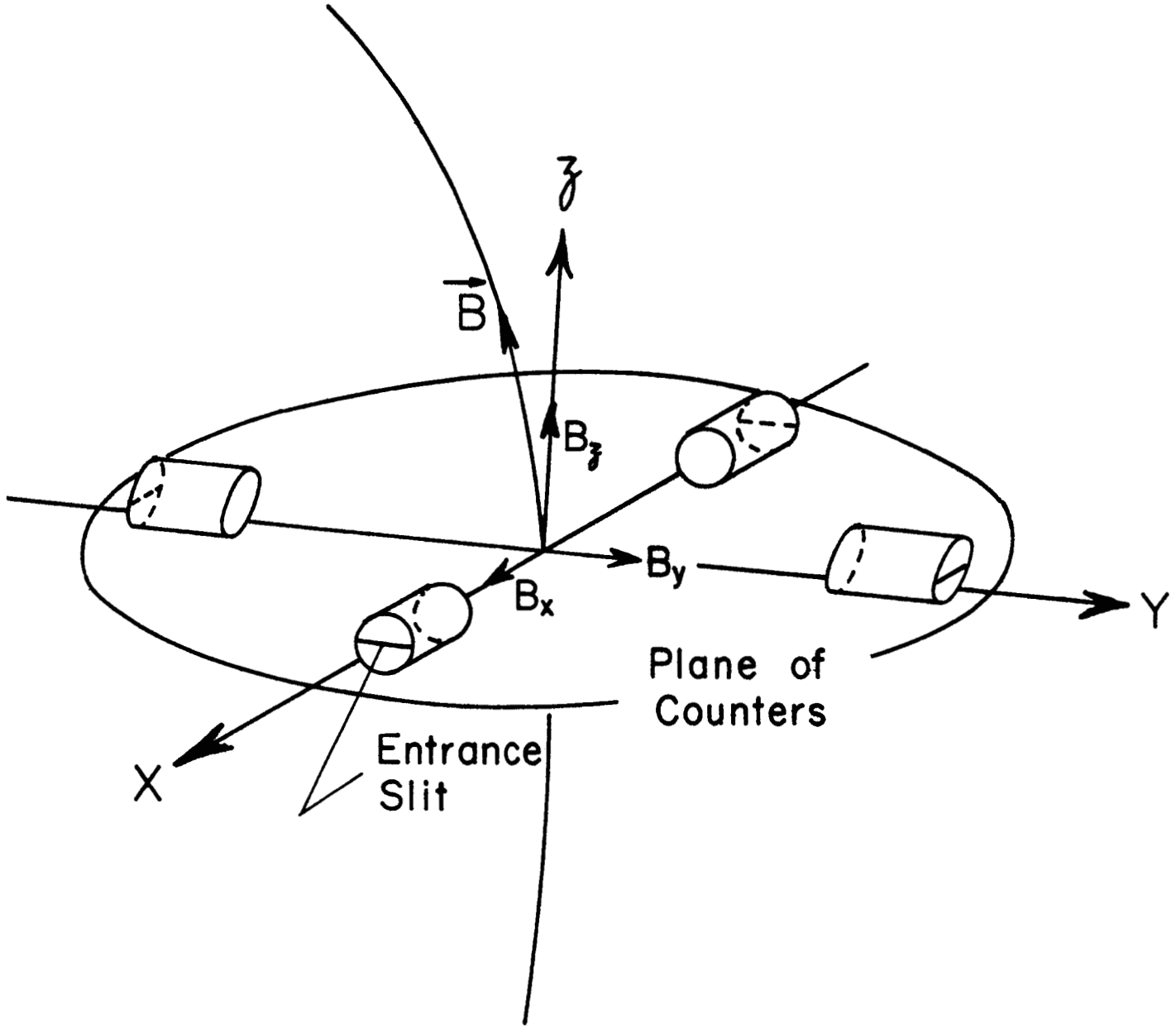

Fig. IV-1. Typical experimental geometry

radiation when this condition is met. Specifically, counting data would be taken when:

a) $\frac{B_z}{(B_x^2+B_y^2+B_z^2)^{1/2}} \gtrsim \cos 30^\circ = 0.866$ — All counters will be within 30° of mirror plane

b) $\frac{B_x(\text{or } B_y)}{(B_x^2+B_y^2+B_z^2)^{1/2}} \gtrsim \cos 30^\circ$ — Counters on y (or x) axis will be within 30° of mirror plane. x (or y) axis counters will point along $\vec{B}$.

Orientation a) would allow measurements of pitch-angle distributions, particle asymmetries and flux. Orientation b) would permit particle flux and asymmetry measurements normal to, and parallel to, the magnetic field, $\vec{B}$. The latter measurement would determine the background count-rate since trapped particles will not have velocities parallel to $\vec{B}$. Pitch angle distributions would not be measured in b).

The specific location and orientation of the counter array in the Apollo spacecraft, e.g. the orbital workshop, need not be specified at the present time. However, there are some general guidelines that can be stated. For long duration missions, and in particular, when the workshop is not occupied by the scientist-astronauts, we may assume that a) the spacecraft will be randomly oriented, and b) the spacecraft establishes itself in a gravity gradient mode. In case a) the orientation of the plane of the counter array with respect to the spacecraft axes is arbitrary, subject to the condition that all counters have an unobstructed field-of-view, i.e. $\pm 10^\circ$ by $\pm 30^\circ$. In case b) gravity-gradient orientation would require that the counter-plane be tilted

approximately 45° with respect to the gradient axis, owing to the fact that the dip angle, I of the magnetic field vector in the South Atlantic anomaly is about 45° (I varies from 30° to 60° in the region where trapped radiation is detected). It is clear that the integration of a flight experiment must take into account the proposed orbit, attitude control, or lack of it, the semi-stable attitude that may be established during extended periods of uncontrolled orientation, and what the motion of the principal axes of the spacecraft might be under these conditions.

We have also looked into the possibility for orienting the experimental package via a magnetically oriented probe. If utilized with a fixed zenith direction in the spacecraft frame of reference, this probe will automatically establish the preferred orientation for the S-16 experiment. A description of the method is as follows:

For definiteness, we shall assume that the probe will be part of an airlock that will be pointed along the local vertical, $\vec{z}$ (see Fig. IV-2). May we first note that orientation and determination of orientation by use of magnetometers have been successfully used in both sounding rocket and balloon applications.[1,2,3] At this time a system using magnetometer controlled gas jets to orient a balloon gondola is currently under construction here at the UC Space Sciences Laboratory.[4]

The method of orientation we are considering here uses the signals from two magnetometers mounted on the experimental package to drive servo motors which rotate the experiment to the required orientation. A Geiger-Müller tube is used to activate and deactivate the mechanism upon entry and exit of the South Atlantic anomaly region. The experimental configuration is shown in Figs. IV-3a,b.

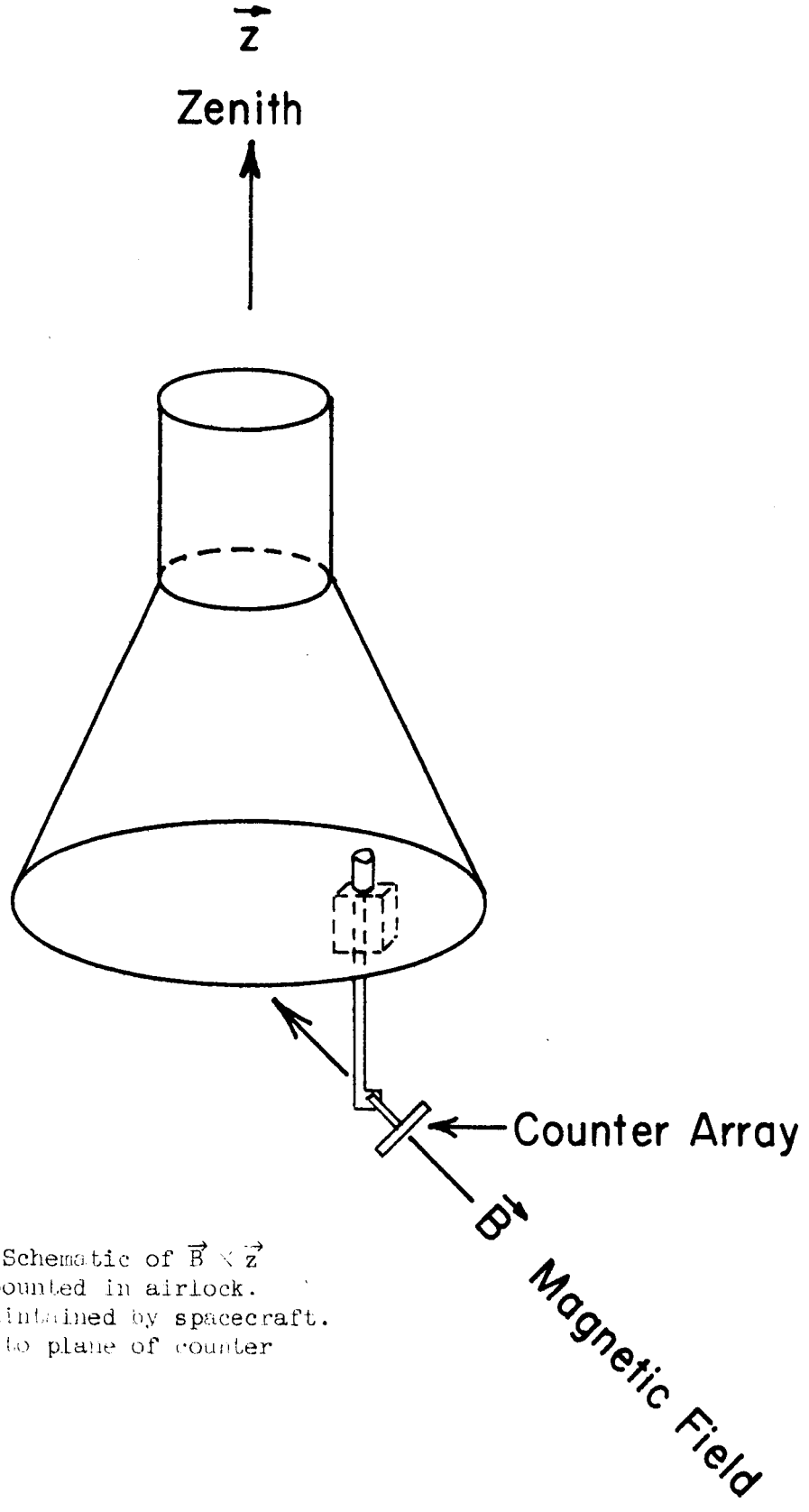

Fig. IV-2. Schematic of $\vec{B} \times \vec{z}$ probe when mounted in airlock. z-axis is maintained by spacecraft. $\vec{B}$ is normal to plane of counter array.

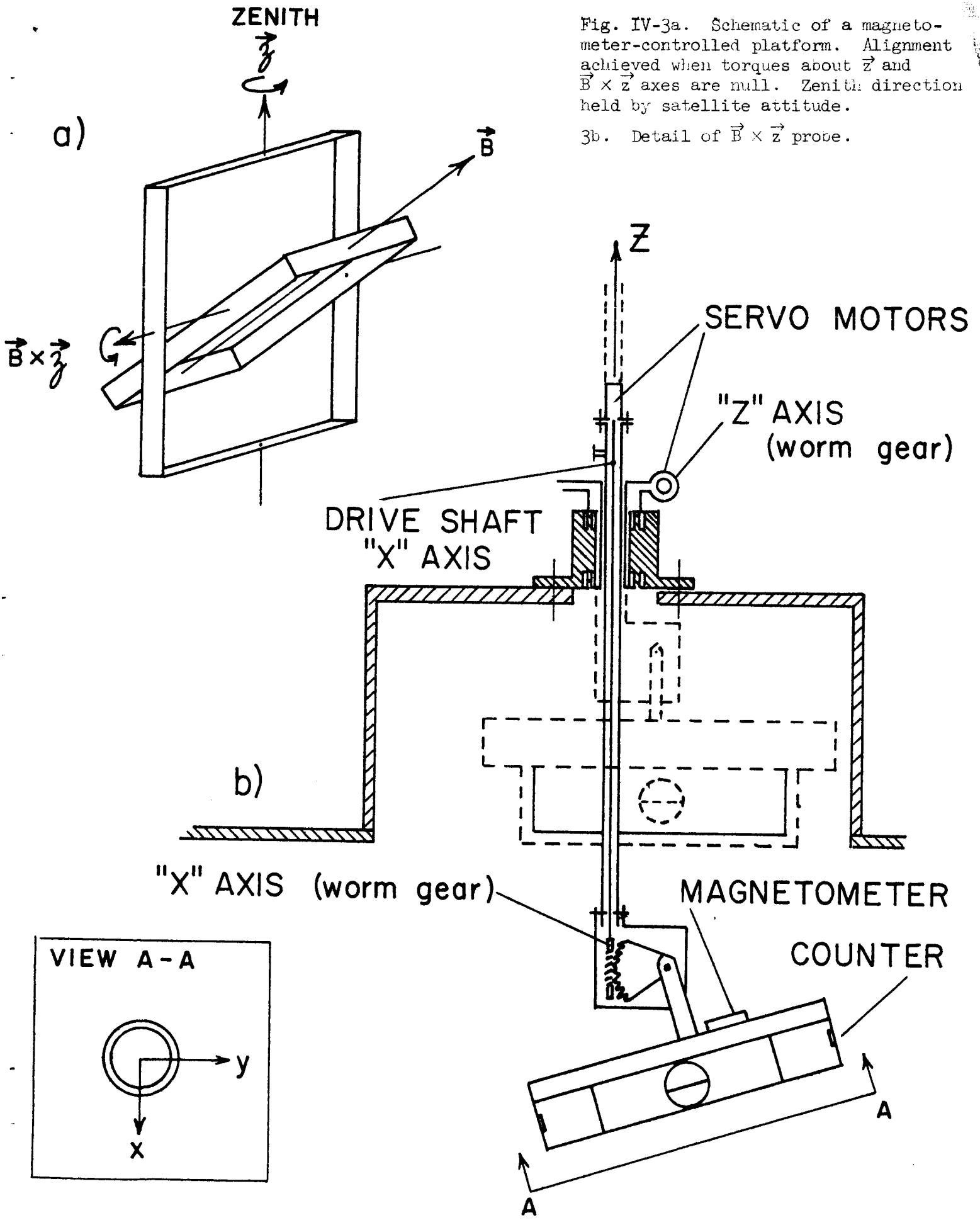

Fig. IV-3a. Schematic of a magnetometer-controlled platform. Alignment achieved when torques about $\vec{z}$ and $\vec{B} \times \vec{z}$ axes are null. Zenith direction held by satellite attitude.

3b. Detail of $\vec{B} \times \vec{z}$ probe.

Nulling the magnetometers mounted along the $\vec{x}$ and $\vec{y}$ axes places the counter array in orientation with $\vec{B}$ perpendicular to the counter plane and places the $\vec{x}$-axis along $\vec{B} \times \vec{z}$, the required orientation.

Electronics: A schematic of the servo circuit and a block diagram of the triggering circuitry are shown in Fig. IV-4. The servo-potentiometers on the shafts provide the signal to return the unit to initial configuration when not in the anomaly. This provides for retrieval through the airlock and also prevents any possible complete rotations of the apparatus.

Standby power of 1 watt is required to keep the GM tube sensitive to the increase in radiation which designates the anomaly region. This standby power could be discontinued when experiment is not going to be done, thus lowering power consumption. Total power consumption is estimated to be from 0.15 to 0.4 kilowatt hours.*

---

* Lower figure assumes a standby of only 6 hours per day, larger is on entire flight.

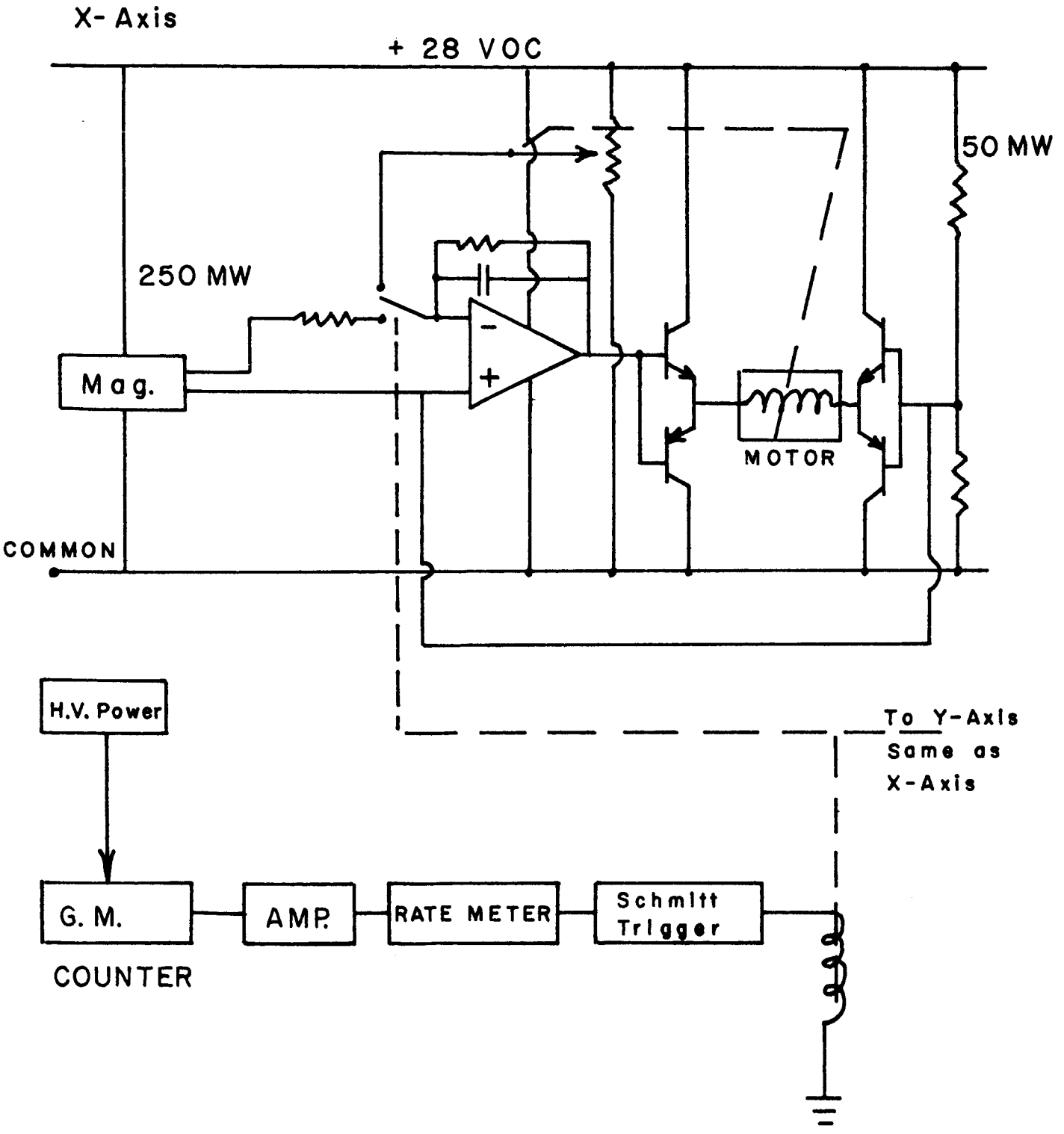

Fig. IV-4. Electronics of $\vec{B} \times \vec{z}$ probe.

C. Flight Unit and Telemetry Requirements

The instrument diagrammatically shown in Fig. IV-5 consists of a solid state counter telescope surrounded by a plastic fluor anti-coincidence detector. Collimation is provided by the telescope-plastic fluor geometry and electronic logic circuitry that selects only particles that deposit energy in the first two solid-state detectors, S_1 and S_2, in time coincidence with one or more of the remaining solid state detectors, S_3-S_8. The geometry defines entrance angles $\pm 6^\circ$ by $\pm 17^\circ$. Dimensions are 4" x 6" x 8". Weight is about 20 pounds.

Shielding is provided by 15 g/cm^2 of lead or tungsten surrounding the plastic fluor and by a 1.8 g/cm^2 aluminum absorber in front of the first solid state detector. The latter provides shielding against the bulk of electron flux below 3 MeV energy and produces relatively little bremmstrahlung. Due to the thin depletion layer (~ 300 microns) and the relatively high bias setting (500 keV), sensitivity of the two front detectors to minimum ionizing electrons and bremmstrahlung is very small. The main purpose of the front aluminum shielding is to avoid signal pile-up in the first solid state detector resulting from the fairly high flux of low energy electrons expected at low L values.

The thin detectors S_1 and S_2 are surface junction solid state detectors which are 300μ thick. S_3-S_8 are lithium drifted solid state detectors each having a depletion thickness of 3 mm and dead layer thickness of about 500μ.

Salient Characteristics of the Flight Instrument

The S-16 particle telescope possesses the following characteristics:

geometric factor - 1.5 (cm^2 ster MeV)

$S_1 = S_2 =$ 1cm x 3cm x 300μ
DIFFUSED JUNC. SILICON DETECTOR

$S_3 = S_4 =$ etc. = 1cm x 3cm x 3mm
LITHIUM DRIFTED
SILICON DETECTOR

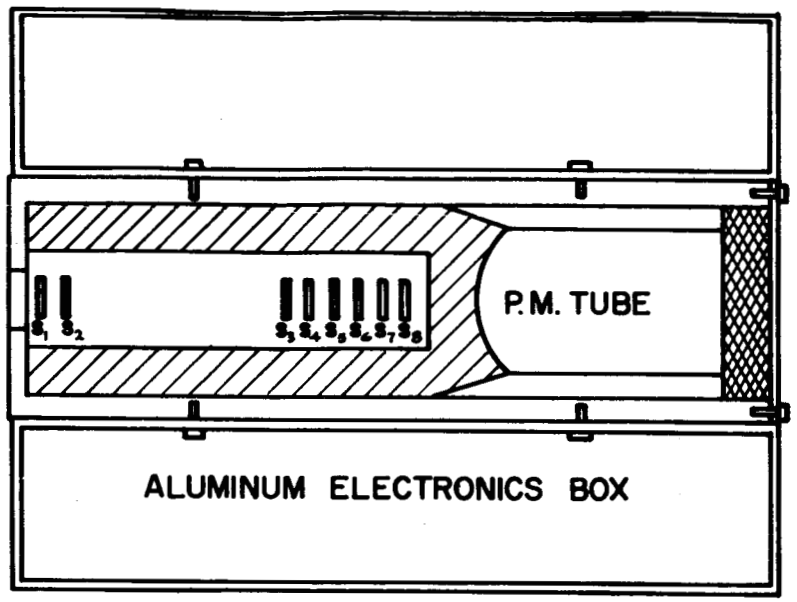

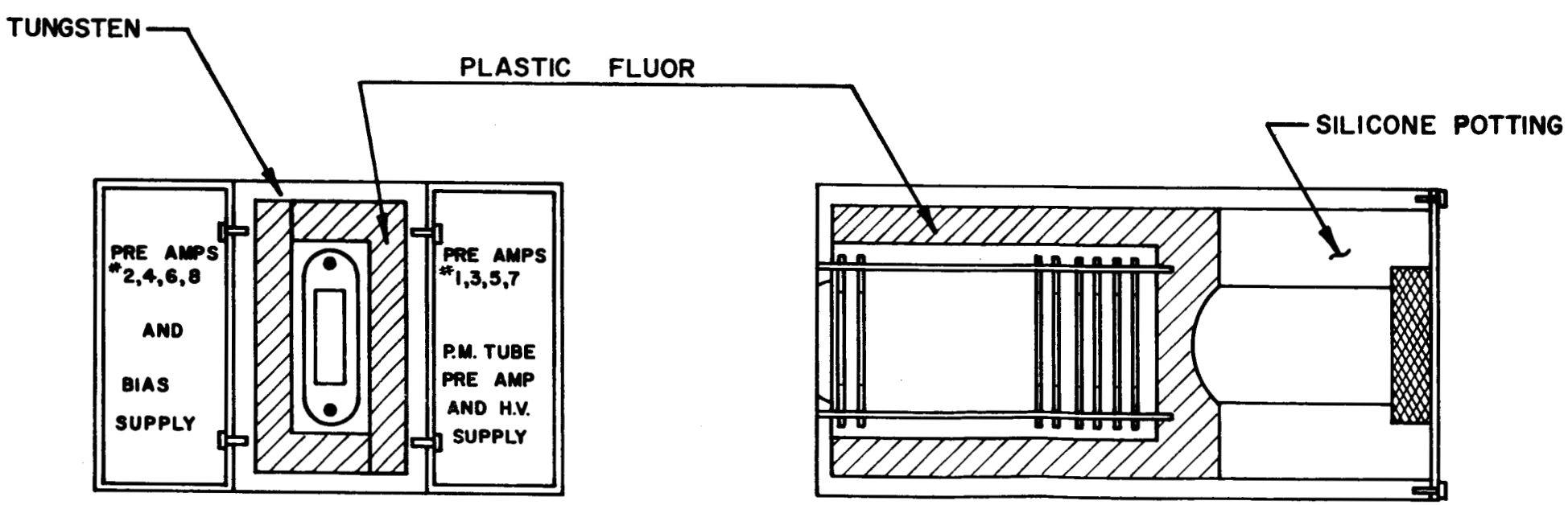

Fig. IV-5

FOLDOUT FRAME 1

FOLDOUT FRAME 2

energy resolution - ~ 2 MeV

pitch angular resolution - $\sigma = \pm \theta/\sqrt{12} = \pm 3.5^{\circ}$, where

$\theta = 12^{\circ}$ rectangular opening

response time - ~ 0.01 millisec/event

dynamic range - 10^5 - 10^6

isotopic separation - ~ 0.1 percent

charge separation - ~ 0.001 percent

lower sensitivity limit - ~ 0.2 prot/cm^2 ster MeV sec

anticipated background rate - ~ 0.1 cps

Low cosmic ray and electron background count rates are achieved by use of lead (tungsten) side shielding and aluminum front shielding for electrons, and an anti-coincidence fluor on the sides. The smallest proton signal expected is about 3 times that for minimum ionizing particles so that counts from cosmic ray particles entering the front and back faces of the instrument are largely rejected by electronic biasing.

Weight and dimensions: Weight of the instrument, shielding, and electronics is 15 to 20 lbs. In addition a cubical volume of 6 inch linear dimensions or its rectangular equivalent is required for the electronic logic circuitry. Location of the latter should be within about 2 feet of the main instrument.

Power requirements: Power consumption for the instrument is approximately 10 watts. The minimum supply voltage required is 24 volts. Maximum supply voltage should not exceed 32 volts.

Maximum count rates in the neighborhood of 1000 counts/sec are expected in the anomaly. This corresponds to a maximum data acquisition

rate of about 64 kilobits/sec for each counter. If four counters are flown, the maximum data acquisition rate is about 250 kilobits/sec. It would be desirable but probably not practical to telemeter at this very high bit rate.

If the data are stored on magnetic tape and then telemetered continuously the bit rate transmission may be reduced by a factor of about 20 to about 12 kilobits/sec which is a more reasonable value. This would require on-board buffer storage of about eight kilocharacters comprising 16 bit words and a tape transport having an acquisition rate of about 16 kilocharacters per second, if two counters are flown. On the basis of this acquisition rate, and the capacity of presently available IBM compatible tapes, each tape would have to be read out at a frequency not less than once a day.

Section IV References

1. Peterson, L. E., A. S. Jacobson and R. M. Pelling, Phys. Rev. Letters, 16, 142, (1966).

2. Peterson, L. E. and A. S. Jacobson, Astrophys. Journ. 145 No. 3, 962 (1966).

3. Bottema, Murk, Applied Optics, Vol. 6, No. 2, 213 (1967).

4. Primbsch, Henry, Private communication.

V. INTERCOMPARISON OF GEOMAGNETIC FIELDS

A final, and important, part of this study was the intercomparison of the several geomagnetic field models now available. The original S-16 experiment employed the use of a computed field direction in order to program the spacecraft attitude as a function of geographic coordinates. We found in this study that the latest GSFC (12/66) field model gave the best fit to surface and satellite field measurements as to magnitude and temporal changes. We believe the vector directions of the field can be accurately calculated to ~ $\pm 1^{\circ}$ uncertainty.

A result of this work was the following paper, titled "B-L Space and Geomagnetic Field Models", to be published in Journal of Geophysical Research, June 1, 1968.

B-L SPACE AND GEOMAGNETIC FIELD MODELS

Peter J. Lindstrom

Space Sciences Laboratory
University of California
Berkeley, California

and

Harry H. Heckman

Lawrence Radiation Laboratory
University of California
Berkeley, California

September 19, 1967

ABSTRACT

We have intercompared geomagnetic field models in B-L space for $0.20 \leq B \leq 0.24$ gauss and $1.2 \leq L \leq 1.8$ R_e (earth radii). Three field models were selected because of their general usage in the analysis of trapped radiation data: Jensen and Whitaker (569 coefficient); Jensen and Cain (48 coefficient); GSFC (9/65)(99 coefficient). These models were compared with the GSFC (12/66) field model (120 coefficient). The geographic coordinates of constant B-L traces were computed using the GSFC (12/66) field in both the southern and northern hemispheres. At each geographical point along the traces thus defined, B and L values were recalculated using different geomagnetic field models. We find that variations in B-L space of the 48- and 569-coefficient models with respect to the 120-coefficient model are great enough to cause significant ambiguities in flux contours of the trapped radiation. We also have examined the effects of temporal variations of the geomagnetic

field on B-L space. The uncertainties in the proton flux contours in B-L space caused by errors in the field models and time variations of the geomagnetic field demonstrate the need for careful reevaluation of existing data that pertain to possible time variations of inner-belt protons. The GSFC (12/66) appears to be sufficiently accurate to undertake such reevaluation.

INTRODUCTION

Since its inception, B-L space has been used extensively in the study of radiation trapped in the earth's magnetic field. B-L space is a two-dimensional, longitude and hemisphere independent, coordinate system, developed by McIlwain, [1961], in which the omnidirectional flux of geomagnetically trapped radiation can be mapped. The B-L coordinate system is applicable to fields that do not possess large azimuthal asymmetries, thereby limiting its use to $L \tilde{<} 5\ R_e$ in the geomagnetic field. Stone [1963] has shown that the B-L coordinates for mirroring particles accurately reflect the invariant shells (I, B_m) describing the adiabatic invariants of charged particle motion [Northrop and Teller, 1960]. Theoretically, particle flux measurements may be reduced and compared accurately in B-L space. However, a geomagnetic field model must be used in the calculation of B and L, and errors dependent on the model can be significant. If the geomagnetic field model used in calculating B and L does not accurately describe the earth's magnetic field, then a real mirror point trajectory will not be represented by a point in B-L space. Flux mapping in such a poorly defined B-L coordinate system would depend on the longitude and the hemisphere where the data were obtained, and the utility of such a B-L system would break down in regions of steep flux gradients. In order to study variations of measured particle fluxes in B-L space, it is necessary to know the variations which could be introduced by the generating geomagnetic field model.

A number of geomagnetic field models are available for the

calculation of B and L values. We have selected the following four field models for the present study:

1. The Jensen and Whitaker 569-coefficient spherical-harmonic expansion model (JW) [Jensen and Whitaker, 1960, Dudziak, et al., 1963];

2. The Jensen and Cain 48-coefficient model (JC) [Jensen and Cain, 1962];

3. The GSFC (9/65) 99-coefficient model [Hendricks and Cain, 1966];

4. The GSFC (12/66) 120-coefficient model [Cain et al., 1967a].

We chose the first three field models because of their use in the analyses of trapped-radiation data. The JW model, for instance, was used in the reduction of the Explorer 4 flux data [McIlwain, 1961]. The JC model is considered to be the standard field model for the interpretation of trapped-particle data [Walt, 1966]. Both the JW and and JC models are static, constructed to represent the geomagnetic field in 1955 and 1960 respectively. The GSFC (9/65) model contains first-time derivatives in the first 48 coefficients and is more accurate than the JW and JC models [Hendricks and Cain, 1966]. The GSFC (12/66) field is the latest field model, and was constructed from OGO-2 satellite magnetic-field measurements as well as the data used in the construction of GSFC (9/65). The GSFC (12/66) contains both first- and second-time derivatives in all its coefficients. Actually, there are two sets of coefficients labeled GSFC (12/66) -- Sets I and II. Both sets were constructed in the same manner using semi-independent samples of the same data. We have chosen arbitrarily to use Set I for our study.

We have limited our study to the region in B-L space bounded by $0.20 \leq B \leq 0.24$ gauss and $1.2 \leq L \leq 1.8$ R_e (earth radii). The lower portion of the inner radiation belt is contained in this interval of B-L values. The gradient of the trapped-particle flux is large along B in this region [Valerio, 1964], and small errors in the computation of B can result in significant errors in the calculated particle flux. In this B-L region, ionization and nuclear collision in the atmosphere are the dominant particle loss mechanisms. The solar cycle changes in the atmosphere will affect changes in particle loss rates, and, hence, particle fluxes. Any valid observation of such changes in the particle flux and loss rates with respect to the solar cycle must clearly take account of the accuracy of the flux representations.

Cain, et al. [1965, 1966, 1967a, b] have made direct comparisons of the JC, GSFC (9/65) and GSFC (12/66) field models with the earth's magnetic field over all longitudes and latitudes. It is concluded by Cain, et al., [1967) that the best current model of the main geomagnetic field is the GSFC (12/66). Excluding OGO-2 satellite data, this model fits the magnetic survey measurements to an accuracy of $\sigma = \pm 122\gamma$, ($1\gamma = 10^{-5}$ gauss) where σ is the standard deviation of the residuals of a random 10% of all survey observations (since 1900). This result is to be compared with the accuracies of the GSFC (9/65) and JC models, $\sigma = \pm 220\gamma$ and $\pm 440\gamma$ [Cain, 1966], respectively. However, when a separate distribution of the residuals is calculated for the OGO-2 data, Cain et al. [1967a] find that the GSFC (12/66) field reproduces the OGO-2 data to $\sigma = \pm 11.7\gamma$. Cognizant of the fact that there are possibilities for systematic errors in the satellite data of the order 10-20γ, Cain et al. [1967a] finally conclude that the surface field is probably no further in error than a few tens of gammas.

Of particular relevance to the analysis of particle data is the

character of the geomagnetic field in the South Atlantic anomaly. The anomaly is not only the site of large particle flux gradients, but also is the region where the relative variations of the selected geomagnetic field models are greatest. For this reason, we examined this specific region for intercomparing the four field models within the range of B-L values we are considering. We obtained from the U. S. Coast and Geodetic Survey magnetic-field measurements taken in the region of the South Atlantic anomaly (-60° to 0° longitude, -45° to -15° latitude) for the period 1900-1965. OGO-2 satellite measurements were included in the set. Computed values of the geomagnetic field, B, were compared with the survey data points for each field model. The mean difference and standard deviation from the mean were computed for the following periods:

a) 1900 through 1963,

b) 1955 through 1963, and

c) 1965.

The results appear in Table I.

Because we are concerned here with the relative accuracies of the models, we did not weight the U. S. Coast and Geodetic Survey data with respect to reliability of the types of geomagnetic field measurements, nor did we invoke a rejection level to eliminate anomalously high deviations in the data. For 1955 through 1963, the GSFC (9/65) and GSFC (12/66) models describe the anomaly region equally well. For 1900 through 1963 GSFC (12/66) is the best model, and the importance of the second time derivatives in the coefficients is clearly evident. We conclude, therefore, that the GSFC (12/66) field model exhibits the highest accuracy of the several models studied within the anomaly

region. Not unexpectedly, the results tabulated in Table I confirm the general conclusions of Cain, et al. [1967a].

The above comparisons of the errors in the magnitude of the geomagnetic field are not, however, a sufficient measure of the model-dependent errors in B-L space. Since a point in B-L space represents the trajectory of the mirror points of a particle trapped in the geomagnetic field, it is necessary to compare the geomagnetic field models over complete B-L traces to reveal the differences that may exist between field models. On the basis of the above discussion, we have selected the GSFC (12/66) field model as the reference field with which the other models were compared. We have made this comparison by (a) calculating the geographic coordinates at various longitudes for a given point in B-L space in the northern and southern hemispheres, as defined by the GSFC (12/66) model, and (b) calculating B and L values for these particular geographic coordinates as computed by the other spherical-harmonic field expansions.

By performing step (b) with the GSFC (12/66), the differences between the given B-L trace and that derived in (b) can be attributable to computational errors only. We find that the maximum computational error in this procedure is ± 10γ in B and ± 0.0005 R_e in L. These errors correspond to a 1-2 kilometer maximum error in locating geographic coordinates given prefixed values of B and L.

METHOD

Using the GSFC (12/66) field model, we calculated sets of geographic coordinates of B-L traces for B values of 0.20 to 0.24 gauss in steps of 0.01 gauss and L values of 1.2 to 1.8 R_e in steps of 0.2 R_e.

We generated these sets for the years 1955 to 1975 in 5-year steps for both the northern and southern hemispheres. The geographic contours were calculated for a given B and L value at 10° intervals in longitude, and in the South Atlantic anomaly region at 5 and 2.5° intervals. By holding B, L, and longitude constant and searching for the altitude and latitude, we located geographic coordinates of a B-L trace with a variation of the computer program SHELL [Roederer and Herod, 1966]. For the computation of B and L we used the computer program INVAR, expanding the subroutine NEWMAG to handle the JW coefficients [McIlwain, 1966]. Given the geographic coordinates computed for the sets of B-L traces defined by the GSFC (12/66) model, we calculated new B and L values using other field models. We have compared the JW and JC fields with the GSFC (12/66) model, both for the years they represent (1955 for JW, 1960 for JC) and for ten years later; and GSFC (9/65) with GSFC (12/66) for 1955, 1965, and 1975. We used GSFC (12/66) for 1965 as the reference field for an examination of the time dependence of the geomagnetic field.

RESULTS

Using the method described above, we made 560 comparisons between the various field representations for selected B-L points in the interval $0.20 \leq B \leq 0.24$ gauss and $1.2 \leq L \leq 1.8$ R_e, respectively. Figure 1 illustrates one of these comparisons. Plotted are the B and L values computed using the JC model for the geographic coordinates of the B(0.24)-L(1.4) mirror-point trajectory defined by the GSFC (12/66) model for 1960. Figure 1 is typical of all of the comparisons we

made because there is no function that will transfer a point in B-L space generated by one geomagnetic field model into a point in B-L space generated by another field model, unless the longitude and hemisphere are known. In other words, flux contours in B-L space cannot be corrected for model-dependent errors without knowing where the data were collected. The flux contours in Fig. 1 are 40 to 110-MeV proton flux contours from INJUN 3 [Valerio, 1964] and are given to indicate the possible range of flux values that can be assigned to the same B-L point.

Let us consider a specific example. Assuming that the INJUN 3 flux contours accurately reflect the shape of the proton flux in the inner radiation belt, then the flux at B = 0.24 gauss, L = 1.4 R_e is 30 protons/cm^2 sec (f_o). If proton flux data were collected in the southern hemisphere at 325° longitude and B-L values were calculated using the JC model, the flux value of f_o would be assigned to the point B = 0.235 gauss L = 1.41 R_e. Owing to this (downward) shift in the flux contours, the "expected" flux value at B = 0.24 gauss, L = 1.4 R_e would be approximately 5 protons/cm^2sec. If in another flight experiment, flux data were collected at 0° longitude in the southern hemisphere, then f_o would be at B = 0.243 gauss, L = 1.386 R_e, and the flux contour would be shifted (upward) so that the flux expected at B = 0.24 gauss, L = 1.4 R_e would be 75 protons/cm^2sec. In the two above cases, the apparent 1:15 ratio in flux values at B = 0.24 gauss, L = 1.4 R_e is due only to relative inaccuracies in the JC field model. We find that the B-L contours, such as Fig. 1, change slowly with

position of the generating B-L point and can be considered to be constant within $\Delta B = \pm 0.01$ gauss and $\Delta L = \pm 0.05$ R_e of the generating point.

Table II gives the maximum deviation in B and L for three examples of B-L points for various field comparisons. The comparison of GSFC (9/65) with GSFC (12/66) confirms the conclusion drawn from the comparisons of these fields with direct geomagnetic-field measurements in the South Atlantic anomaly region -- namely, that the two models agree quite well for 1965 but diverge from each other 10 years before or after. The comparisons between JC and GSFC (12/66) show large variations at all B-L points studied in both 1960, the year the JC field model was generated to represent, and 10 years later. The variations between JW and GSFC (12/66) are even larger.

Table II also shows the range of proton-flux values as deduced from the INJUN 3 proton-flux contours, which could be assigned to the same B-L point due to errors in the geomagnetic-field model. We note that the flux variations caused by errors in the JW and JC fields are comparable to the magnitude of flux changes expected over a solar cycle [Blanchard and Hess, 1964].

The comparison of GSFC (12/66) for 1965 with GSFC (12/66) for 1955 and for 1975 shows another factor which must be taken into consideration in studies of the temporal changes of the trapped radiation. Figure 2 is a comparison of GSFC (12/66) for 1965 with GSFC (12/66) for 1975 at B = 0.24 gauss, L = 1.4 R_e. The magnitude of the variation in B-L space of the same geographic coordinates over a 10-year period shows that the geomagnetic field is dynamic. Trapped radiation flux

contours constructed in B-L space can contain significant errors if the field model used does not represent the geomagnetic field at the time the data were collected. An important feature of the time variations of the geomagnetic field with respect to the trapped radiation is the change in altitude of the same B-L trace in the South Atlantic anomaly region. Figure 3 shows the B-L trace of $L = 1.4\ R_e$, $B = 0.22$ and 0.24 gauss for 1965 and for 1975. Over a 10-year period the minimum mirror-point altitude at $L = 1.4\ R_e$, $B \geq 0.20$ gauss decreases about 70 kilometers. Particles mirroring at the same B and L values will experience a denser atmosphere in 1975 than in 1965. The flux of trapped radiation at $L = 1.4\ R_e$ and $B = 0.23$ gauss will decrease by about a factor of four, and at $B = 0.24$ gauss will virtually disappear in 10 years, independent of solar activity. The problems introduced by the time dependence of minimum mirror-point altitudes cannot be circumvented by the use of a static field model because of the nature of temporal variations (Fig. 2). The geomagnetic field must be treated as a dynamic field for any long-range studies and predictions of trapped radiation.

The plots of the geomagnetic field comparisons listed in Table II are available in University of California Space Sciences Laboratory Report Series 8 Issue 69, "B-L Space and Geomagnetic Field Models". These plots can be used in converting flux data in B-L space defined by one geomagnetic-field model into B-L space defined by another, provided geographic positions of the flux measurements are known.

CONCLUSION

Model-dependent errors can cause large apparent differences in trapped particle fluxes in B-L space. There is no simple way to transform

B-L points of one field model to B-L points of another field model without using the geographic coordinates used in generating the B-L points. Temporal variations of the geomagnetic field alter the geographic positions of mirror-point trajectories. Since the dominant particle-loss mechanisms for the region of B-L space studied are ionization and nuclear collision in the atmosphere, any computation of loss rates, lifetimes, and temporal changes of particles in the inner belt strongly depends on the use of an accurate time-dependent geomagnetic-field model. The range of model-dependent errors in B-L space demonstrates the need for careful reevaluation of existing data that pertain to possible time variations of inner-belt particle fluxes.

It is our opinion that the GSFC (12/66) field model may possess sufficient accuracy to warrant its use for generating B-L coordinates in such reevaluation. However, the analysis of particle flux data in regions of large flux gradients requires accuracies in the computed values of B that are of the order ± 40 to 50γ. Whether or not this accuracy is actually attained by the GSFC (12/66) model requires experimental confirmation. The intercomparison of the GSFC (12/66) field with the results of the Cosmos 26 and 49 satellites in the South Atlantic anomaly [Cain, Langel, and Hendricks, 1967b] gives partial confirmation for the accuracy of "a few tens of gammas" in the GSFC (12/66) field.

We have shown that the GSFC (9/65) and (12/66) field models describe the geomagnetic field, epoch 1965, in the South Atlantic anomaly equally well. We note, however, that the 99-coefficient GSFC (9/65) field expansion pre-dates the OGO-2 data, yet, fits the OGO-2 observations in the South Atlantic anomaly to an accuracy $\sigma = \pm 14.5\gamma$ (Table I).

Thus, we believe there is evidence that the GSFC (12/66) field model describes the geomagnetic field for epoch 1965 to the desired accuracy of about ± 50γ. Improvements in the secular variations of the coefficients will, in all probability, require updating as later field measurements become available. It is therefore essential that trapped particle data be readily accessible in their original geographic coordinates to allow for any further reevaluation of the data should subsequent improvements in the representation of the geomagnetic field require it.

ACKNOWLEDGMENT

This work was done under the auspices of the U. S. Atomic Energy Commission and the National Aeronautics and Space Administration Contract 9-5249.

REFERENCES

Blanchard, R. C., and W. N. Hess, Solar cycle changes in inner-zone protons, J. Geophys. Res., 69, 3927-3938, 1964.

Cain, J.C., W. E. Daniels, S. J. Hendricks, and D. C. Jensen, An Evaluation of the main geomagnetic field 1940-1962, J. Geophys. Res., 70, 3647-3674, 1965.

Cain, J. C., Models of the earth's magnetic field, in Radiation trapped in the earth's magnetic field, pp 7-25, DeReidel Publishing Company, Dordrecht, Holland, 1966

Cain, J. C., S. J. Hendricks, R. A. Langel, and W. V. Hudson, A proposed model for the international geomagnetic reference field, 1965, Preprint, Goddard Space Flight Center, Greenbelt, Maryland, 1967a.

Cain, J. C., R. A. Langel, S. J. Hendricks, Magnetic chart of the Brazilian anomaly -- a verification, Preprint, Goddard Space Flight Center, Greenbelt, Maryland, 1967b.

Dudziak, W. F., D. C. Kleinecke, T. J. Kostigen, Tabular displays of geomagnetic geometry, RM 63TMP-3, DASA 1377, Tempo, General Electric Company, Santa Barbara, California, 1963.

Hendricks, S. J., and J. C. Cain, Magnetic field data for trapped particle evaluations, J. Geophys. Res., 71, 346-347, 1966.

Jensen, D. C., and J. C. Cain, An interim geomagnetic field, J. Geophys. Res., 67, 3568-3569, 1962.

Jensen, D. C., and W. A. Whitaker, A spherical harmonic analysis of the geomagnetic field, J. Geophys. Res., 65, 2500, 1960.

McIlwain, C. E., Coordinates for mapping the distribution of geomagnetically trapped particles, J. Geophys. Res., 66, 3681-3692, 1961.

McIlwain, C. E., private communication, 1966.

Northrop, T. G., and E. Teller, Stability of the adiabatic motion of charged particles in the earth's field, Phys. Rev., 117, 215-225, 1960.

Roederer, J. G., and J. V. Herod, A computational model for geomagnetically trapped particle shells and kinematic parameters, Air Force Weapons Laboratory Technical Report No. AFWL-TR-66-78, Air Force Systems Command, Kirtland Air Force Base, New Mexico, 1966.

Stone, E. C., The physical significance and application of L, B_o and R_o to geomagnetically trapped particles, J. Geophys. Res., 68, 4157-4166, 1963.

Valerio, J., Protons from 40 to 110 MeV observed on Injun 3, J. Geophys. Res. 69, 4949-4958, 1964.

Walt, M., Future magnetic field for B-L space, in Radiation trapped in the earth's magnetic field, p. 62, DeReidel Publishing Company, Dordrecht, Holland, 1966.

Table I. Mean deviation and standard deviation between unweighted magnetic survey data and computed values in the region of the South Atlantic anomaly.

Field model	Number of data points	Mean deviation (γ)	Standard deviation (γ)
Surface and air 1900-1963 geomagnetic-field measurements			
JW	1369	-155.6	1056.3
JC		-560.2	892.0
GSFC (9/65)		297.0	477.6
GSFC (12/66)		-1.2	180.0
Surface and air 1955-1963 geomagnetic-field measurements			
JW	825	461.2	524.4
JC		-20.4	301.5
GSFC (9/65)		15.2	177.2
GSFC (12/66)		9.7	171.9
OGO-2 satellite measurements			
GSFC (9/65)	1330	7.1	14.5
GSFC (12/66)		1.8	7.2

Table II Geomagnetic comparisons of various field model configurations for three B-L points.

B_1 (gauss)	L_1 (R_e)	Year for GSFC(12/66) used in generating B_1-L_1 trajectory	Field for evaluating B-L at geographic coordinates of B_1-L_1 trajectory	Range of differences $\pm\Delta L$, between L and L_1		Range of differences $\pm\Delta B$, between B and B_1		Range of INJUN 3 proton fluxes (J = particles/cm^2 sec allowed by errors in B-L space	
				$+\Delta L$ ($10^{-4} R_e$)	$-\Delta L$ ($10^{-4} R_e$)	$+\Delta B$ (γ)	$-\Delta B$ (γ)	J max	J min
0.21	1.2	1955	GSFC (9/65) for 1955	16	16	61	36	160	130
		1965	GSFC (9/65) for 1965	16	12	37	39	160	140
		1975	GSFC (9/65) for 1975	39	62	149	84	170	130
		1960	JC	91	94	122	208	190	90
		1970	JC	148	190	545	222	310	110
		1955	JW	69	127	685	378	290	70
		1965	JW	77	217	739	440	350	70
		1965	GSFC (12/66) for 1955	75	158	504	107	300	120
		1965	GSFC (12/66) for 1975	199	62	105	600	170	40
0.24	1.4	1955	GSFC (9/65) for 1955	30	33	105	89	35	25
		1965	GSFC (9/65) for 1965	26	16	45	42	30	30
		1975	GSFC (9/65) for 1975	106	83	163	160	40	20
		1960	JC	135	148	416	544	75	5
		1970	JC	323	358	830	211	180	20
		1955	JW	213	312	1028	596	170	5
		1965	JW	230	385	1366	662	325	0
		1965	GSFC (12/66) for 1955	227	323	628	181	140	20
		1965	GSFC (12/66) for 1975	379	226	181	613	45	0
0.24	1.8	1955	GSFC (9/65) for 1955	39	47	119	63	125	110
		1965	GSFC (9/65) for 1965	32	31	51	79	120	110
		1975	GSFC (9/65) for 1975	165	117	288	285	140	95
		1960	JC	121	192	603	584	160	80
		1970	JC	444	468	1189	108	200	105
		1955	JW	363	440	706	605	170	80
		1965	JW	274	439	1110	678	200	75
		1965	GSFC (12/66) for 1955	350	433	693	174	160	105
		1965	GSFC (12/66) for 1975	481	377	180	816	130	75

FIGURE CAPTIONS

1. Longitudinal contours of B and L values for the northern and southern hemispheres computed with the 3C (48 coefficient) field model given the geographic coordinates of the mirror point trajectory, B = 0.24 gauss and L = 1.4 R_e, defined by the GSFC (12/66) field, epoch 1960. Longitude is indicated at 30° intervals, and the South Atlantic anomaly is identified by the shaded area. Injun 3 proton flux contours, 40 < E < 110 MeV, are indicated.

2. Temporal change of B and L coordinates over a 10 year period, computed using the GSFC (12/66) field, epoch 1975 given the geographic coordinates of the mirror point trajectory B = 0.24 gauss and L = 1.4 R_e defined by the GSFC (12/66) field, epoch 1965. Longitude is indicated at 10° intervals.

3. Temporal changes in typical B L traces in the region of the South Atlantic anomaly, computed using the GSFC (12/66) field for epochs 1965 and 1975.

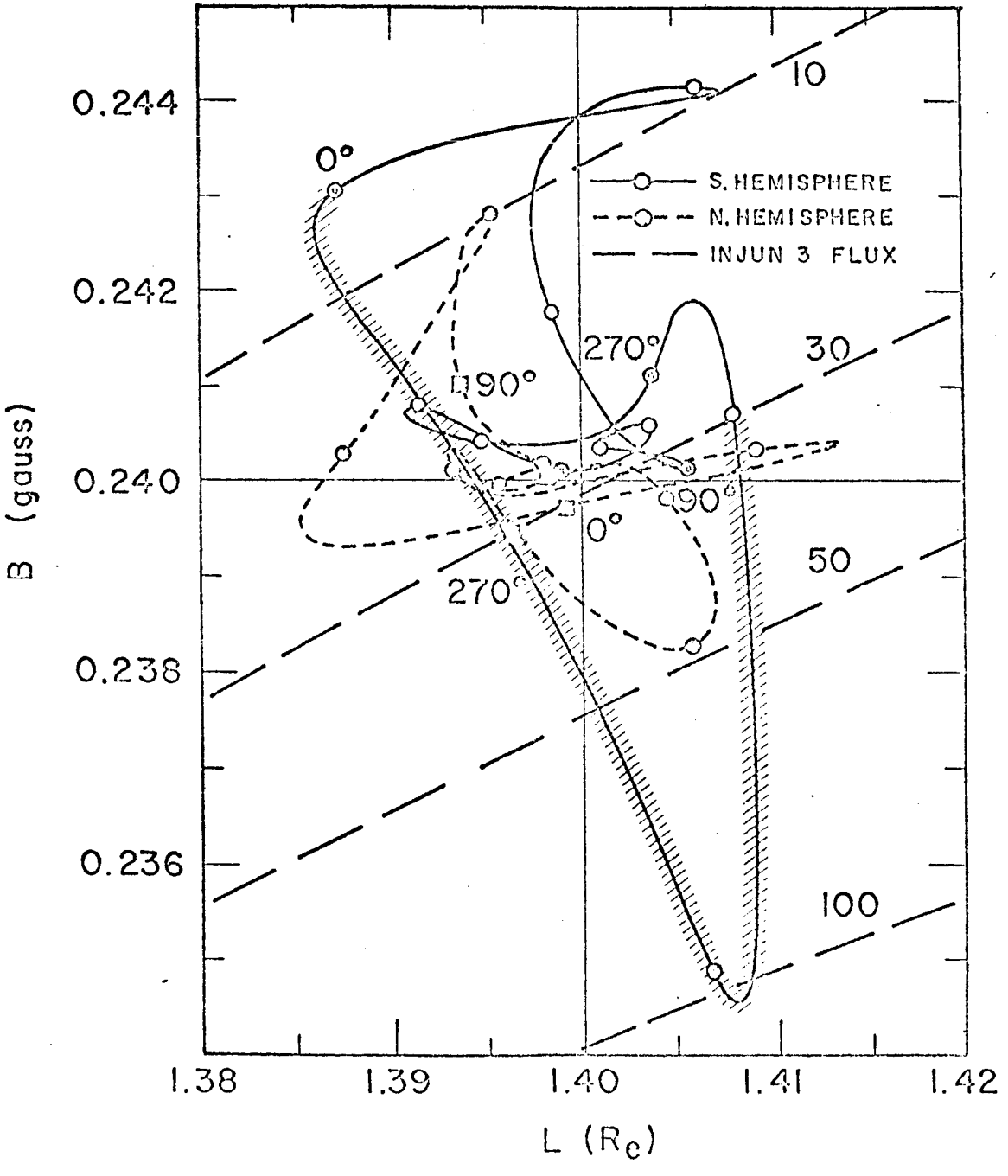

XBL 670-5311-A

Fig. 1

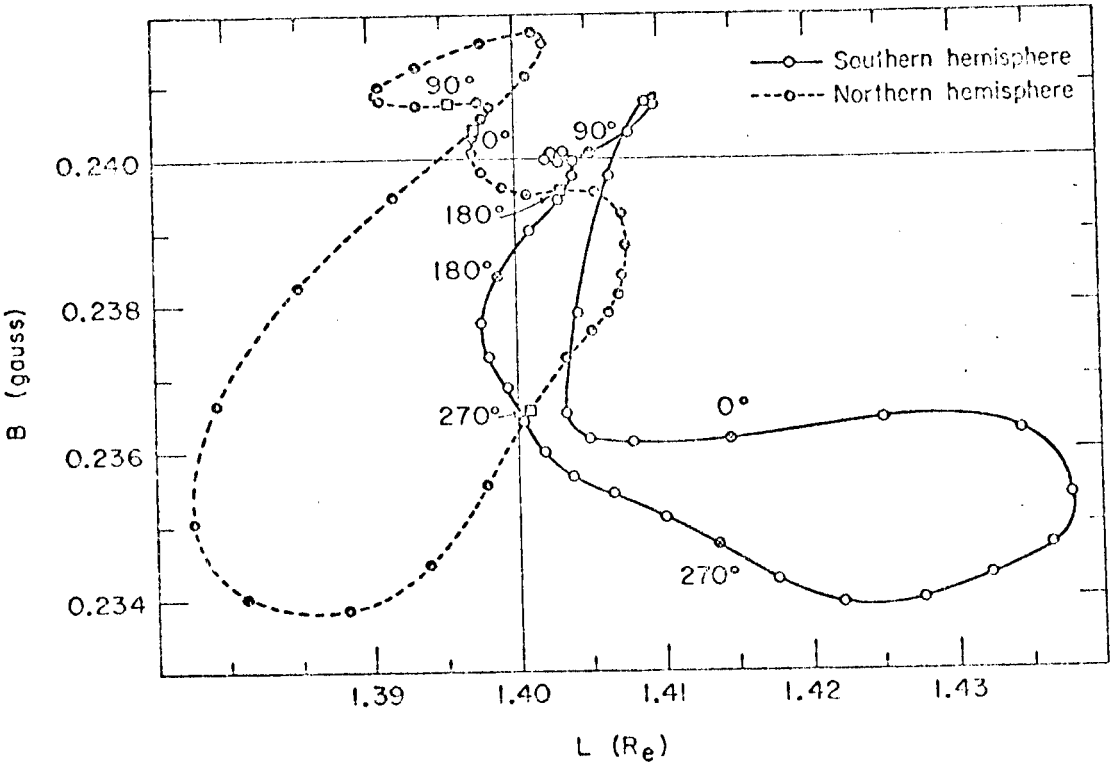
Southern hemisphere
Northern hemisphere
90°
0°
90°
180°
180°
270°
0°
270°
0.240
0.238
0.236
0.234
B (gauss)
1.39
1.40
1.41
1.42
1.43
L (Re)
XBL670-5314

Fig. 2

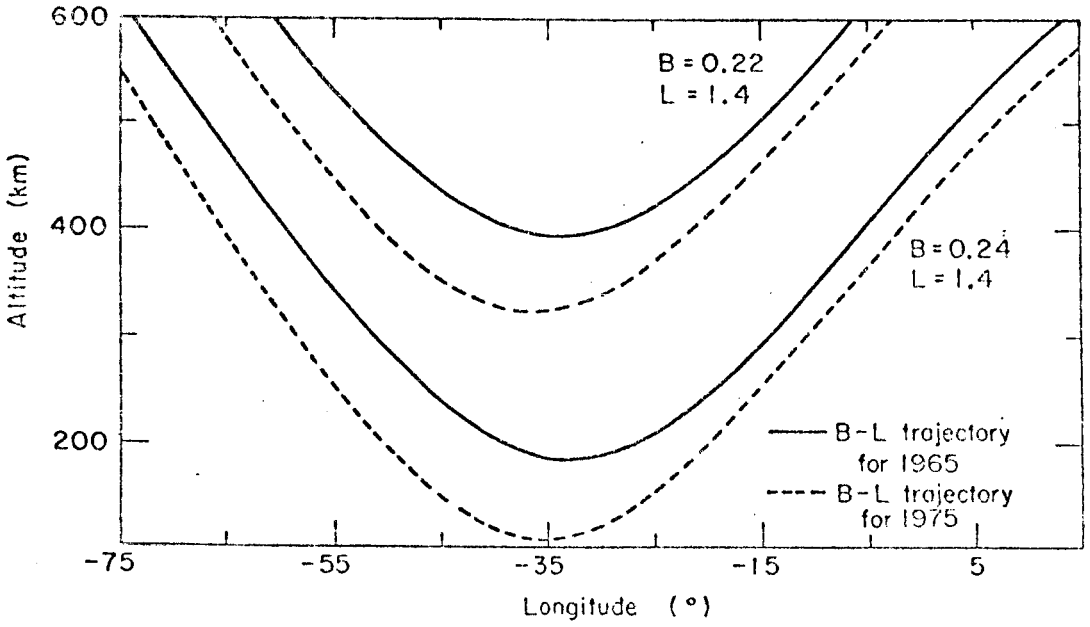

XBL 670-5315

Fig. 3